Title	Theoretical elucidation of space charge effects on the coupled-bunch instability at the 3 GeV Rapid Cycling Synchrotron at the Japan Proton Accelerator Research Complex
Author(s)	Shobuda Yoshihiro, Chin Y. H., Saha P. K., Hotchi Hideaki, Harada Hiroyuki, Irie Yoshiro, Tamura Fumihiko, Tani Norio, Toyama Takeshi, Watanabe Yasuhiro, Yamamoto Masanobu
Citation	Progress of Theoretical and Experimental Physics, 2017(1), p.013G01_1-013G01_39
Text Version	Publisher
URL	https://jopss.jaea.go.jp/search/servlet/search?5057702
DOI	https://doi.org/10.1093/ptep/ptw169
Right	Originally published in Progress of Theoretical and Experimental Physics, 2017, 1, 013G01 © The Author(s) 2017. Published by Oxford University Press on behalf of the Physical Society of Japan. This is an Open Access article distributed under the terms of the Creative Commons Attribution License (http://creativecommons.org/licenses/by/4.0/), which permits unrestricted reuse, distribution, and reproduction in any medium, provided the original work is properly cited.

PTEP

Prog. Theor. Exp. Phys. **2017**, 013G01 (39 pages)
DOI: 10.1093/ptep/ptw169

Theoretical elucidation of space charge effects on the coupled-bunch instability at the 3 GeV rapid cycling synchrotron at the Japan Proton Accelerator Research Complex

Yoshihiro Shobuda[1,*], Yong Ho Chin[2], Pranab Kumar Saha[1], Hideaki Hotchi[1], Hiroyuki Harada[1], Yoshiro Irie[2], Fumihiko Tamura[1], Norio Tani[1], Takeshi Toyama[1], Yasuhiro Watanabe[1], and Masanobu Yamamoto[1]

[1]*J-PARC Center, JAEA&KEK, 2-4 Shirakata, Tokaimura, Nakagun, Ibaraki 319-1195, Japan*
[2]*KEK, 1-1 Oho, Tsukuba, Ibaraki 305-0801, Japan*
[*]E-mail: yoshihiro.shobuda@j-parc.jp

Received June 22, 2016; Revised October 28, 2016; Accepted November 1, 2016; Published January 21, 2017

The Rapid Cycling Synchrotron (RCS), whose beam energy ranges from 400 MeV to 3 GeV and which is located in the Japan Proton Accelerator Research Complex, is a kicker-impedance-dominated machine, which violates the impedance budget from a classical viewpoint. Contrary to conventional understanding, we have succeeded in accelerating a 1 MW equivalent beam. The machine has some interesting features: e.g., the beam tends to be unstable for the smaller transverse beam size and the beam is stabilized by increasing the peak current. Space charge effects play an important role in the beam instability at the RCS. In this study, a new theory has been developed to calculate the beam growth rate with the head-tail and coupled-bunch modes (m, μ) while taking space charge effects into account. The theory sufficiently explains the distinctive features of the beam instabilities at the RCS.

Subject Index G11

1. Introduction

The 3 GeV Rapid Cycling Synchrotron (RCS) at the Japan Proton Accelerator Research Complex [1] aims to achieve a megawatt-class beam. Two bunched beams (4.15×10^{13} particles per bunch) are accelerated from 400 MeV to 3 GeV with a repetition rate of 25 Hz. To avoid the effects of eddy currents on metal chambers [2,3], ceramic chambers are adopted instead [4,5]. Accordingly, the resistive wall impedance [5–10] is negligible in the RCS [11–13].

However, there has been some concern that the kicker impedance limits the beam intensity of the RCS [14] by exciting beam instabilities [6]. Precise offline and online measurements of the impedance show that the kicker at the RCS has a huge impedance [15]. The offline measurement is conducted using the standard wire method [7], while the online one is conducted by observing the beam induced-voltage at the end of the power cable [15]. The results of these two independent measurements agree with each other. Finally, we demonstrate that the RCS is a kicker-impedance-dominated machine; we show this by suppressing the beam growth rate in accordance with the reduction of the kicker impedance [12,13].

In general, when we design accelerators, a lower impedance source along the rings is preferable for achieving a high intensity beam. Concretely, ceramic chambers are adopted, the chambers are connected as smoothly as possible over the rings [16], and significant efforts are made to lower the kicker impedances [12,17].

The conventional Sacherer formula [18,19] estimates the beam growth rate by using the impedances as an input parameter. However, such estimation differs significantly from the measured results at the RCS. We suspected the main reason for this is that the formula neglects space charge effects. Because the RCS covers the intermediate energy region (from 400 MeV to 3 GeV), space charge should have an effect on the beam instability.

Other theories exist to assess beam instability that includes space charge effects [20–22]. However, those theories assume simple forms of impedance, e.g., resistive wall impedance, resonator type impedance with a single resonance frequency, and constant wakes. Moreover, the theories do not include coupled-bunch-type instabilities.[1]

In this paper, we develop a new theory that includes coupled-bunch and head-tail instabilities with space charge effects based on the Vlasov equation [6,23]. Using this theory, we try to understand the parameter dependence (the transverse emittance dependence, the beam peak current dependence, the tune dependence, etc.) of the beam instability observed at the RCS.

In Sect. 2, we start with the Hamiltonian and construct the Vlasov equation [6]. In Sect. 2.1, we derive a dispersion relation with the head-tail and coupled-bunch modes (m, μ) that includes space charge effects. In Sect. 2.2, we reproduce the previous Sacherer formula by neglecting the space charge effects.

In Sect. 3, typical parameters at the RCS are shown, and we show that the observed beam instability cannot be explained at all using the classical theory, i.e., Sacherer's theory [18,19], where space charge effects are neglected.

In Sect. 4, the beam instability observed at the RCS is analyzed using our new theory. In Sect. 4.1, the space charge effects on the beam instability are investigated by comparing the measurements with the theoretical results. In Sect. 4.2, tune manipulations are discussed from both the theoretical and the experimental viewpoints. The paper is summarized in Sect. 5.

In Appendix A, the scalar potential describing the space charge effect is calculated by solving the Poisson equation with the boundary condition of being surrounded by a perfectly conductive cylindrical chamber. In Appendix B, we explain canonical transformations to derive the Hamiltonian describing nonlinear betatron oscillation by using action-angle variables from the original Hamiltonian given by Eq. (1) in the next section.

2. Linearized Vlasov approach

The linearized Vlasov approach is a standard theoretical method to analyze beam instabilities [6]. In Sect. 2.1, the linearized Vlasov equation converts to a dispersion relation as a powerful tool to discuss the space charge effect on the beam instability. In Sect. 2.2, the classical Sacherer formula is reproduced, based on the linearized Vlasov equation.

[1] After this paper had been submitted on 22 June 2016, the authors attended the 57th ICFA Advanced Beam Dynamics Workshop on High-Intensity and High-Brightness Hadron Beams (HB2016: https://hb2016.esss.se/) and found that A. Burov had submitted a document entitled "Coupled-beam and coupled-bunch instabilities" to http://arxiv.org/pdf/1606.07430v1.pdf on 27 June 2016. He discusses the space charge effect on coupled-bunch-type instabilities by another approach.

2.1. Dispersion relation with the head-tail and coupled-bunch modes that include space charge effects

Here, we present the dispersion relation, by which we calculated the beam growth rate; this method takes into account the coupled mode μ, head-tail mode m, and space charge effects.

The original Hamiltonian is given by [24,25]

$$\begin{aligned} H_o = &-p_s\left(1+\frac{x}{\rho}\right)\frac{\Delta E}{p_s\beta_s c}+\frac{p_s}{2\gamma_s^2}\left(\frac{\Delta E}{p_s\beta_s c}\right)^2+\frac{p_x^2+p_y^2}{2p_s}+\frac{p_s}{2}K_x(s)\left(1-\frac{\Delta E}{E_s}\right)x^2 \\ &+\frac{p_s}{2}K_y(s)\left(1-\frac{\Delta E}{E_s}\right)y^2-\frac{p_s x}{E_s}F_x+\frac{e\Phi_c(x,y,s-c\beta_s t)}{\beta_s\gamma_s^2 c} \\ &-\frac{eV_{\rm rf}}{\omega_{\rm RF}}\delta_p(s)\cos\left(\omega_{\rm RF}t-\frac{hs}{R}+\varphi_s\right)+\ldots, \end{aligned} \tag{1}$$

where φ_s is the synchronous phase; p_s is the constant longitudinal momentum of the synchronous particle; $E_s = cp_s/\beta_s$ is the particle energy on the designed orbit; β_s and γ_s are the Lorentz-β and the Lorentz-γ of the designed particle, respectively; ΔE is given by $\Delta E = E - E_s$; F_x is the transverse wake force; $\delta_p(s)$ is the periodic δ-function; c is the velocity of light; K_x and K_y are the periodic focusing forces in the horizontal and the vertical directions, respectively; Φ_c is the space charge potential felt by the bunch center [26]; h is harmonic number; $V_{\rm rf}$ is the amplitude of the radio frequency (RF) voltage; $1/\rho$ is the local curvature around the machine; R is the average radius of the machine; and $\omega_{\rm RF}$ is the angular frequency of the RF voltage, which is expressed as

$$\omega_{\rm RF} = \frac{c\beta_s h}{R}. \tag{2}$$

The orbit length s is used as an independent variable. The canonical variables are (x, p_x), (y, p_y), and $(t, -E)$ for the horizontal, vertical, and longitudinal directions, respectively. The scalar potential Φ_c is obtained by solving the Poisson equation with the boundary condition that the beam is surrounded by a cylindrical, perfectly conductive chamber with radius a. The solution is expressed in Appendix A.

Successive canonical transformations convert Eq. (1) to the Hamiltonian with action-angle variables, to describe the nonlinear betatron motions. The derivation is explained in detail in Appendix B. From now on, we consider only the horizontal and the longitudinal motions of the beam, for simplicity. Finally, the Hamiltonian is given by

$$H \simeq Q_x J_x + \nu_{s0} J_L + U_x + Y', \tag{3}$$

with the horizontal (J_x, ψ_x) and the longitudinal action-angle variables (J_L, ϕ_L), and its independent variable $\theta = s/R$, where Q_x and ν_{s0} are the horizontal and the synchrotron tunes, and

$$U_x = -\frac{2\beta_s R}{c}\left(\left(\frac{\beta_x(s)J_x}{2p_s}\right)^{1/2}\cos\left(\psi_x+\phi_x(s)-\frac{Q_x}{R}s\right)-\frac{D(s)}{\beta_s}\left(\frac{\omega_0\nu_{s0}J_L}{2E_s|\eta|}\right)^{1/2}\cos\phi_L\right)F_x, \tag{4}$$

$$\phi_x(s) = \int^s \frac{ds}{\beta_x(s)}, \tag{5}$$

$$Y' = Y'_{\rm coh,0}(J_L) + Y'_{\rm coh,2}(J_L)\frac{\beta_x(s)J_x}{p_s} + Y'_{\rm coh,4}(J_L)\frac{3\beta_x^2(s)J_x^2}{2}, \tag{6}$$

$$Y'_{\mathrm{coh},0}(J_L) = \frac{eRZ_0eN_b\left(\tilde{\gamma} - \mathrm{Ei}[-\frac{a^2}{2\sigma_x^2}] + \log[\frac{a^2}{2\sigma_x^2}]\right)}{4\pi^2\beta_s\gamma_s^2\sigma_z}\left(\frac{\pi}{2}\right)^{1/2}\exp\left(-\frac{c^2J_L|\eta|}{2E_sh^2\nu_{s0}\sigma_z^2\omega_0}\right)$$
$$\times I_0\left(\frac{c^2J_L|\eta|}{2E_sh^2\nu_{s0}\sigma_z^2\omega_0}\right), \tag{7}$$

$$Y'_{\mathrm{coh},2}(J_L) = -\frac{eRZ_0eN_b}{8\pi^2\beta_s\gamma_s^2\sigma_x^2}\left(\frac{\pi}{2}\right)^{1/2}\exp\left(-\frac{c^2J_L|\eta|}{2E_sh^2\nu_{s0}\sigma_z^2\omega_0}\right)\Bigg[-\frac{\sigma_x^2(\tilde{\gamma} - \mathrm{Ei}[-\frac{a^2}{2\sigma_x^2}] + \log[\frac{a^2}{2\sigma_x^2}])}{2\gamma_s^2\sigma_z^5}$$
$$\times\left(\left(\sigma_z^2 - \frac{c^2J_L|\eta|}{E_sh^2\nu_{s0}\omega_0}\right)I_0\left(\frac{c^2J_L|\eta|}{2E_sh^2\nu_{s0}\sigma_z^2\omega_0}\right) + \frac{c^2J_L|\eta|I_1(\frac{c^2J_L|\eta|}{2E_sh^2\nu_{s0}\sigma_z^2\omega_0})}{E_sh^2\nu_{s0}\omega_0}\right)$$
$$+\left(1 - \exp\left(-\frac{a^2}{2\sigma_x^2}\right)\right)\frac{I_0(\frac{c^2J_L|\eta|}{2E_sh^2\nu_{s0}\sigma_z^2\omega_0})}{\sigma_z}\Bigg] + \frac{eRZ_0eN_b\exp\left(-\frac{c^2J_L|\eta|}{2E_sh^2\nu_{s0}\sigma_z^2\omega_0}\right)}{4\sqrt{2\pi}\pi\beta_s\gamma_s^2\sigma_x^4\sigma_z}$$
$$\times\left(\sigma_x^2 + \frac{2\sigma_x^4\left(\exp\left(-\frac{a^2}{2\sigma_x^2}\right) - 1\right)}{a^2}\right)I_0\left(\frac{c^2J_L|\eta|}{2E_sh^2\nu_{s0}\sigma_z^2\omega_0}\right)$$
$$-\frac{eRZ_0eN_b}{8\pi^2\beta_s\gamma_s^2\sigma_x^2\sigma_z}\left(\frac{\pi}{2}\right)^{1/2}\exp\left(-\frac{c^2J_L|\eta|}{2\sigma_z^2h^2\omega_0E_s\nu_{s0}}\right)I_0\left(\frac{c^2J_L|\eta|}{2\sigma_z^2h^2\omega_0E_s\nu_{s0}}\right), \tag{8}$$

$$Y'_{\mathrm{coh},4}(J_L)$$
$$= -\frac{eRZ_0eN_b\exp\left(-\frac{c^2J_L|\eta|}{2E_sh^2\nu_{s0}\sigma_z^2\omega_0}\right)}{16\pi^2\sigma_x^2\beta_s\gamma_s^2p_s^2}\left(\frac{\pi}{2}\right)^{1/2}\Bigg\{-\frac{\sigma_x^2\left(\tilde{\gamma} - \mathrm{Ei}[-\frac{a^2}{2\sigma_x^2}] + \log[\frac{a^2}{2\sigma_x^2}]\right)}{2}$$
$$\times\Bigg[\frac{\left(3\sigma_z^4 - \frac{6c^2J_L\sigma_z^2|\eta|}{E_sh^2\nu_{s0}\omega_0} + \frac{2c^4J_L^2|\eta|^2}{E_s^2h^4\nu_{s0}^2\omega_0^2}\right)I_0(\frac{c^2J_L|\eta|}{2E_sh^2\nu_{s0}\sigma_z^2\omega_0}) - \frac{2c^2J_L|\eta|\left(-2\sigma_z^2 + \frac{c^2J_L|\eta|}{E_sh^2\nu_{s0}\omega_0}\right)I_1(\frac{c^2J_L|\eta|}{2E_sh^2\nu_{s0}\sigma_z^2\omega_0})}{E_sh^2\nu_{s0}\omega_0}}{8\gamma_s^4\sigma_z^9}$$
$$-\frac{(\sigma_z^2 - \frac{c^2J_L|\eta|}{E_sh^2\nu_{s0}\omega_0})I_0(\frac{c^2J_L|\eta|}{2E_sh^2\nu_{s0}\sigma_z^2\omega_0}) + \frac{c^2J_L|\eta|I_1(\frac{c^2J_L|\eta|}{2E_sh^2\nu_{s0}\sigma_z^2\omega_0})}{E_sh^2\nu_{s0}\omega_0}}{\sigma_x^2\gamma_s^2\sigma_z^5} + \frac{I_0(\frac{c^2J_L|\eta|}{2E_sh^2\nu_{s0}\sigma_z^2\omega_0})}{\sigma_x^4\sigma_z}\Bigg]$$
$$+\left[1 - \exp\left(-\frac{a^2}{2\sigma_x^2}\right) - \tilde{\gamma} + \mathrm{Ei}[-\frac{a^2}{2\sigma_x^2}] - \log[\frac{a^2}{2\sigma_x^2}]\right]$$
$$\times\left[\frac{(\sigma_z^2 - \frac{c^2J_L|\eta|}{E_sh^2\nu_{s0}\omega_0})I_0(\frac{c^2J_L|\eta|}{2E_sh^2\nu_{s0}\sigma_z^2\omega_0}) + \frac{c^2J_L|\eta|}{E_sh^2\nu_{s0}\omega_0}I_1(\frac{c^2J_L|\eta|}{2E_sh^2\nu_{s0}\sigma_z^2\omega_0})}{2\gamma_s^2\sigma_z^5} - \frac{I_0(\frac{c^2J_L|\eta|}{2E_sh^2\nu_{s0}\sigma_z^2\omega_0})}{\sigma_x^2\sigma_z}\right]$$
$$+\frac{(6 - (\frac{a^2}{\sigma_x^2} + 6)\exp\left(-\frac{a^2}{2\sigma_x^2}\right) - 4\tilde{\gamma} + 4\,\mathrm{Ei}[-\frac{a^2}{2\sigma_x^2}] - 4\log[\frac{a^2}{2\sigma_x^2}])I_0(\frac{c^2J_L|\eta|}{2E_sh^2\nu_{s0}\sigma_z^2\omega_0})}{8\sigma_x^2\sigma_z}\Bigg\}$$

$$
+\frac{eRZ_0eN_b\exp\left(-\frac{c^2J_L|\eta|}{2E_sh^2\nu_{s0}\sigma_z^2\omega_0}\right)}{8\pi^2\sigma_x^4\beta_s\gamma_s^2p_s^2}\left(\frac{\pi}{2}\right)^{1/2}
$$

$$
\times\left\{\frac{(8\sigma_x^2-\exp\left(-\frac{a^2}{2\sigma_x^2}\right)(\frac{a^4}{\sigma_x^2}+4a^2+8\sigma_x^2))I_0(\frac{c^2J_L|\eta|}{2E_sh^2\nu_{s0}\sigma_z^2\omega_0})}{4a^2\sigma_z}\right.
$$

$$
+\sigma_x^2\left[2\sigma_x^2-(a^2+2\sigma_x^2)\exp\left(-\frac{a^2}{2\sigma_x^2}\right)\right]\left[\left(\frac{1}{4\sigma_x^2}+\frac{1}{a^2}\right)\frac{I_0(\frac{c^2J_L|\eta|}{2E_sh^2\nu_{s0}\sigma_z^2\omega_0})}{\sigma_x^2\sigma_z}\right.
$$

$$
\left.\left.-\frac{(\sigma_z^2-\frac{c^2J_L|\eta|}{E_sh^2\nu_{s0}\omega_0})I_0(\frac{c^2J_L|\eta|}{2E_sh^2\nu_{s0}\sigma_z^2\omega_0})+\frac{c^2J_L|\eta|I_1(\frac{c^2J_L|\eta|}{2E_sh^2\nu_{s0}\sigma_z^2\omega_0})}{E_sh^2\nu_{s0}\omega_0}}{4a^2\gamma_s^2\sigma_z^5}\right]+\sigma_x^2\left[1-\exp\left(-\frac{a^2}{2\sigma_x^2}\right)\right]\right.
$$

$$
\left.\times\left[-\frac{I_0(\frac{c^2J_L|\eta|}{2E_sh^2\nu_{s0}\sigma_z^2\omega_0})}{\sigma_x^2\sigma_z}+\frac{(\sigma_z^2-\frac{c^2J_L|\eta|}{E_sh^2\nu_{s0}\omega_0})I_0(\frac{c^2J_L|\eta|}{2E_sh^2\nu_{s0}\sigma_z^2\omega_0})+\frac{c^2J_L|\eta|I_1(\frac{c^2J_L|\eta|}{2E_sh^2\nu_{s0}\sigma_z^2\omega_0})}{E_sh^2\nu_{s0}\omega_0}}{4\gamma_s^2\sigma_z^5}\right]\right\}
$$

$$
+\frac{eRZ_0eN_b\exp\left(-\frac{c^2J_L|\eta|}{2E_sh^2\nu_{s0}\sigma_z^2\omega_0}\right)}{32\pi^2\sigma_x^4\beta_s\gamma_s^2\sigma_zp_s^2}\left(\frac{\pi}{2}\right)^{1/2}\left(1-\frac{8\sigma_x^4-\exp\left(-\frac{a^2}{2\sigma_x^2}\right)(4a^2\sigma_x^2+8\sigma_x^4)}{a^4}\right)
$$

$$
\times I_0\left(\frac{c^2J_L|\eta|}{2E_sh^2\nu_{s0}\sigma_z^2\omega_0}\right)+\frac{eRZ_0eN_b}{\beta_s\gamma_s^2\pi^2\sigma_x^2p_s^2}\left(\frac{\pi}{2}\right)^{1/2}\exp\left(-\frac{c^2J_L|\eta|}{2h^2\omega_0E_s\nu_{s0}\sigma_z^2}\right)
$$

$$
\times\left[\left(-\frac{1}{128\gamma_s^2\sigma_z^3}+\frac{1}{64\sigma_x^2\sigma_z}+\frac{c^2J_L|\eta|}{128\gamma_s^2\sigma_z^5h^2\omega_0E_s\nu_{s0}}\right)I_0(\frac{c^2J_L|\eta|}{2h^2\omega_0E_s\nu_{s0}\sigma_z^2})\right.
$$

$$
\left.-\frac{c^2J_L|\eta|I_1(\frac{c^2J_L|\eta|}{2h^2\omega_0E_s\nu_{s0}\sigma_z^2})}{128\gamma_s^2\sigma_z^5h^2\omega_0E_s\nu_{s0}}\right]; \tag{9}
$$

η is slippage factor; $Z_0 = 120\pi\ \Omega$ is the impedance of free space; ω_0 is the angular revolution frequency; $\beta_x(s)$ is the Twiss parameter; $D(s)$ is the dispersion function; $I_n(x)$ is the modified Bessel function; Ei[z] is the exponential integral function [27]; $\tilde{\gamma}$ is Euler-γ; and σ_x and σ_z are the root mean square (rms) horizontal and longitudinal beam sizes, respectively. The potential functions U_x and Y' originate from the horizontal wake and the space charge forces, respectively.

Here, let us consider the situation that M buckets are filled with M bunches in a ring. We denote by $\Psi_n(\theta, J_x, \psi_x, J_L, \phi_L)$ the phase space distribution function of the nth bunch among M bunches.

The Vlasov equation is expressed as

$$
\frac{\partial\Psi_n}{\partial\theta}+J_x'\frac{\partial\Psi_n}{\partial J_x}+\psi_x'\frac{\partial\Psi_n}{\partial\psi_x}\partial\psi_y+J_L'\frac{\partial\Psi_n}{\partial J_L}+\phi_L'\frac{\partial\Psi_n}{\partial\phi_L}=0, \tag{10}
$$

where the prime denotes differentiation with respect to the variable θ.

The distribution function Ψ_n is decoupled into an unperturbed part $F_0(J_x)G_0(J_L)$ and a perturbed part $f_1(J_x,\psi_x)g_1(J_L,\phi_L)$ as

$$\Psi_n = F_0(J_x)G_0(J_L) + f_1(J_x,\psi_x)g_1(J_L,\phi_L)\exp\left(j\nu\theta - j\nu\frac{2\pi n}{M} - j\frac{Q_x\xi_x\phi_{cp}}{h\eta} - j\frac{2\pi\mu n}{M}\right), \quad (11)$$

where $Q_x\xi_x$ is the chromaticity in the horizontal direction and Ψ_n is normalized according to

$$\int_0^\infty dJ_x\int_{-\pi}^{\pi}d\psi_x\int_0^\infty dJ_L\int_{-\pi}^{\pi}d\psi_L\Psi_n(J_x,\psi_x,J_L,\phi_L) = 1. \quad (12)$$

In advance, let us formulate the dipole current Dp of the beam (and its Fourier transform $\tilde{D}(p)$) and the horizontal wake force F_x (i.e., the potential U_x) not only in the time domain but also in the frequency domain. The horizontal wake force F_x is obtained by the summation of the wake force induced by the previous passage of beams. It is expressed as

$$\begin{aligned} F_x = {} & \frac{e^2N_b}{2\pi R}\int_0^\infty dJ_x'\int_{-\pi}^{\pi}d\psi_x'\int_0^\infty dJ_L'\int_{-\pi}^{\pi}d\phi_L'x'f_1(J_x',\psi_x')g_1(J_L',\phi_L') \\ & \times\sum_{n'=0}^{M-1}\sum_{k=-\infty}^{\infty}\exp\left(j\nu\theta + j\nu\left(-\frac{2\pi n'}{M} - 2\pi k\right) - j\frac{Q_x\xi_x\phi_{cp}'}{h\eta}\right)\exp\left(-j\frac{\mu 2\pi n'}{M}\right) \\ & \times W_T\left(\frac{\phi_{cp}'}{h} - \frac{\phi_{cp}}{h} + 2\pi k + \frac{2\pi(n'-n)}{M}\right), \end{aligned} \quad (13)$$

where $W_T(s)$ is the horizontal wake function, which has the causality condition $W_T(s) = 0$ for $s \le 0$, and ϕ_{cp} denotes the longitudinal position of beam, which is related to J_L and ϕ_L as

$$\phi_{cp} = \left(\frac{2J_Lh^2|\eta|\omega_0}{cp_s\beta_s\nu_{s0}}\right)^{1/2}\sin\phi_L, \quad (14)$$

(see Eq. (B31)). The effect of the wake excited by all previous revolutions of beams is included as a summation over k in Eq. (13). The dipole current Dp, its Fourier transform $\tilde{D}(p)$, and the horizontal impedance $Z_T(\omega)$ are defined as

$$Dp(J_L,\phi_L) = \int_0^\infty dJ_x\int_{-\pi}^{\pi}d\psi_x\frac{x(J_x,\psi_x,J_L,\phi_L)f_1(J_x,\psi_x)g_1(J_L,\phi_L)}{\sqrt{\beta_x}}, \quad (15)$$

$$\tilde{D}(p) = \frac{1}{2\pi}\int_0^\infty dJ_L\int_{-\pi}^{\pi}d\phi_LDp(J_L,\phi_L)\exp\left(jp\frac{\phi_{cp}}{h}\right), \quad (16)$$

and

$$W_T(\omega_0t) = -\int_{-\infty}^{\infty}\frac{d\omega}{2\pi}jZ_T(\omega)\exp\left(j\frac{\omega}{\omega_0}\omega_0t\right), \quad (17)$$

respectively, where

$$\begin{aligned} x(J_x,\psi_x,J_L,\phi_L) = {} & \left(\frac{2\beta_x(s)J_x}{p_s}\right)^{1/2}\cos(\psi_x + \phi_x(s) - Q_x\theta) \\ & - \frac{D(s)}{p_sc}\left(\frac{2\nu_{s0}\omega_0E_sJ_L}{|\eta|}\right)^{1/2}\cos\phi_L, \end{aligned} \quad (18)$$

and j is the imaginary unit (the definitions of the causality condition of the wake function and of the impedance in Ref. [6] are different from those in this paper (see Eqs. (13) and (17))).

Substituting Eqs. (15) and (17) into Eq. (13) and using Poisson's sum rule [6],

$$\sum_{k=-\infty}^{\infty} \exp(jkx) = 2\pi \sum_{p=-\infty}^{\infty} \delta(x - 2\pi p), \tag{19}$$

where $\delta(x)$ is the δ-function, the wake force F_x is rewritten as

$$\begin{aligned} F_x = &-\frac{je^2 N_b \sqrt{\beta_x}}{T_0 R} \exp\left(j\nu\theta - j\nu\frac{2\pi n}{M}\right) \sum_{n'=0}^{M-1} \sum_{p=-\infty}^{\infty} \tilde{D}\left(\nu + p - \frac{Q_x \xi_x}{\eta}\right) \\ &\times \exp\left(-j\frac{2\pi\mu n'}{M} + jp\frac{2\pi(n'-n)}{M}\right) Z_T(\omega_0(Q_x + p)) \exp\left(-j(\nu+p)\frac{\phi_{cp}}{h}\right), \end{aligned} \tag{20}$$

in frequency domain, where T_0 is the revolution time of the designed particle. Now, the potential U_x in Eq. (4) can be expressed as

$$\begin{aligned} U_x = &\frac{je^2 N_b \beta_s^2 \sqrt{\beta_x}}{\pi R} \exp\left(j\nu\theta - j\nu\frac{2\pi n}{M}\right) \\ &\times \left(\left(\frac{\beta_x(s) J_x}{2p_s}\right)^{1/2} \cos\left(\psi_x + \phi_x(s) - \frac{Q_x}{R}s\right) - \frac{D}{\beta_s}\left(\frac{\omega_0 \nu_{s0} J_L}{2E_s|\eta|}\right)^{1/2} \cos\phi_L\right) \\ &\times \sum_{n'=0}^{M-1} \sum_{p=-\infty}^{\infty} \tilde{D}\left(\nu + p - \frac{Q_x\xi_x}{\eta}\right) \exp\left(-j\frac{2\pi\mu n'}{M} + jp\frac{2\pi(n'-n)}{M}\right) \\ &\times Z_T(\omega_0(\nu+p)) \exp\left(-j(\nu+p)\frac{\phi_{cp}}{h}\right). \end{aligned} \tag{21}$$

Second, we introduce the Fourier transforms of the perturbed parts f_1 and g_1 as

$$f_1(J_x, \psi_x) = \sum_q \tilde{f}_{1,q}(J_x) \exp(-jq\psi_x), \tag{22}$$

$$g_1(J_L, \phi_L) = \sum_m \tilde{g}_{1,m}(J_L) \exp(-jm\phi_L). \tag{23}$$

Substituting Eqs. (22)–(23) into Eq. (15), the dipole current Dp is rewritten as

$$\begin{aligned} &Dp(J_L, \phi_L) \\ &= \sum_{q',m'} \int_0^{\infty} dJ_x \int_{-\pi}^{\pi} d\psi_x \frac{x(J_x, \psi_x, J_L, \phi_L) \tilde{f}_{1,q'}(J_x) \tilde{g}_{1,m'}(J_L)}{\sqrt{\beta_x}} \exp\left(-jq'\psi_x - jm'\phi_L\right). \end{aligned} \tag{24}$$

Here, we introduce $Dp_{q',l',m'}(J_L)$ as

$$Dp(J_L,\phi_L) = \sum_{q',m'} Dp_{q',m'}(J_L)\exp\left(-jm'\phi_L\right), \tag{25}$$

so that

$$\begin{aligned} Dp_{q',m}(J_L) = &\sum_{m'}\int_{-\pi}^{\pi} d\phi_L \int_0^{\infty} dJ_x \int_{-\pi}^{\pi} d\psi_x \\ &\times \tilde{f}_{1,q'}(J_x)\tilde{g}_{1,m'}(J_L)\frac{x(J_x,\psi_x,J_L,\phi_L)}{2\pi\sqrt{\beta_x}}\exp\left(-jq'\psi_x - j(m'-m)\phi_L\right). \end{aligned} \tag{26}$$

Then, Eq. (16) is expanded by $Dp_{q,m}$ as

$$\begin{aligned} \tilde{D}(p) &= \frac{1}{2\pi}\int_0^{\infty} dJ_L \int_{-\pi}^{\pi} d\phi_L Dp(J_L,\phi_L)\exp\left(jp\frac{\phi_{cp}}{h}\right) \\ &= \sum_{q,m}\int_0^{\infty} dJ'_L Dp_{q,m}(J'_L)J^*_m\left[p\frac{\omega_{\mathrm{RF}}}{h}\left(\frac{2J'_L|\eta|}{cp_s\beta_s\nu_{s0}\omega_0}\right)^{1/2}\right], \end{aligned} \tag{27}$$

by using the relation

$$\begin{aligned} \int_{-\pi}^{\pi}\exp\left(-jq\frac{\phi_{cp}}{\omega_{\mathrm{RF}}}+jm\phi_L\right)d\phi_L &= \int_{-\pi}^{\pi}\exp\left(-jq\left(\frac{2J_L|\eta|}{cp_s\beta_s\nu_{s0}\omega_0}\right)^{1/2}\sin\phi_L + jm\phi_L\right)d\phi_L \\ &= 2\pi J_m\left[q\left(\frac{2J_L|\eta|}{cp_s\beta_s\nu_{s0}\omega_0}\right)^{1/2}\right], \end{aligned} \tag{28}$$

where $*$ denotes the complex conjugate and $J_m[x]$ is the Bessel function [27].

The equations of motion are given by

$$\frac{dJ_x}{d\theta} = -\frac{\partial H}{\partial\psi_x}, \tag{29}$$

$$\frac{d\psi_x}{d\theta} = \frac{\partial H}{\partial J_x}, \tag{30}$$

$$\frac{dJ_L}{d\theta} = -\frac{\partial H}{\partial\phi_L}, \tag{31}$$

$$\frac{d\phi_L}{d\theta} = \frac{\partial H}{\partial J_L}, \tag{32}$$

where the Hamiltonian is given by Eq. (3). By substituting Eqs. (11) and (29)–(32) into Eq. (10), and by retaining only the perturbed parts, the linearized Vlasov equation is obtained as

$$\begin{aligned} &\left(j\nu - j\frac{Q_x\xi_x}{h\eta}\nu_L(J_x,J_L)\omega_{\mathrm{RF}}\left(\frac{2|\eta|RJ_L}{\beta_s^3 cE_s\nu_{s0}}\right)^{1/2}\cos\phi_L\right)f_1(J_x,\psi_x)g_1(J_L,\phi_L) \\ &+\frac{je^2N_b\beta_s^2\beta_x(s)}{\sqrt{2p_s}\pi R}\sqrt{J_x}\sin\left(\psi_x+\phi_x(s)-Q_x\theta\right) \\ &\times\sum_{n'=0}^{M-1}\sum_{p=-\infty}^{\infty}\tilde{D}\left(\nu+p-\frac{Q_x\xi_x}{\eta}\right)\exp\left(-j\frac{2\pi\mu n'}{M}+jp\frac{2\pi(n'-n)}{M}\right)Z_T(\omega_0(\nu+p)) \end{aligned}$$

$$\times \exp\left(-j(\nu+p)\frac{\phi_{cp}}{h}\right)\frac{\partial F_0(J_x)}{\partial J_x}G_0(J_L)\exp\left(j\frac{Q_x\xi_x\phi_{cp}}{h\eta}+j\frac{2\pi\mu n}{M}\right)$$
$$+\nu_x(J_x,J_L)\frac{\partial f_1(J_x,\psi_x)}{\partial\psi_x}g_1(J_L,\phi_L)+\nu_L(J_x,J_L)f_1(J_x,\psi_x)\frac{\partial g_1(J_L,\phi_L)}{\partial\phi_L}=0, \tag{33}$$

where we assume

$$\frac{dG_0(J_L)}{dJ_L}\simeq 0, \tag{34}$$

and

$$\nu_L(J_x,J_L)=\nu_{s0}+\frac{dY'}{dJ_L}, \tag{35}$$

$$\nu_x(J_x,J_L)=Q_x+\frac{dY'}{dJ_x}. \tag{36}$$

Here, let us substitute Eqs. (22)–(23) into Eq. (33) before it is multiplied by $\exp\left(jq'\psi_x+jm'\phi_L\right)$. By integrating the result over ψ_x and ϕ_L, we obtain approximately

$$\tilde{f}_{1,q'}(J_x)\tilde{g}_{1,m'}(J_L)$$
$$\simeq j\frac{e^2N_b\beta_s^2\beta_x(s)\sqrt{J_x}(\exp\left(j(\phi_x(s)-Q_x\theta)\right)\delta_{q',-1}-\exp\left(-j(\phi_x(s)-Q_x\theta)\right)\delta_{q',1})\exp\left(j\frac{2\pi\mu n}{M}\right)}{2\sqrt{2p_s}\pi R\left[\nu-m'\nu_L(J_x,J_L)-q'\nu_x(J_x,J_L)\right]}$$
$$\times\sum_{n'=0}^{M-1}\sum_{p=-\infty}^{\infty}\tilde{D}\left(\nu+p-\frac{Q_x\xi_x}{\eta}\right)\exp\left(-j\frac{2\pi\mu n'}{M}+jp\frac{2\pi(n'-n)}{M}\right)Z_T(\omega_0(\nu+p))$$
$$\times J_{m'}\left[\left(\frac{(\nu+p)\omega_{\mathrm{RF}}}{h}-\frac{Q_x\xi_x\omega_{\mathrm{RF}}}{h\eta}\right)\left(\frac{2J_L|\eta|}{cp_s\beta_s\nu_{s0}\omega_0}\right)^{1/2}\right]\frac{\partial F_0(J_x)}{\partial J_x}G_0(J_L), \tag{37}$$

under the condition

$$1\gg\left(-\frac{2\omega_0J_L}{\nu_{0s}\beta_s^2E_s\eta}\right)^{1/2}\frac{|Q_x\xi_x|}{Q_x}\nu_L(J_x,J_L), \tag{38}$$

where we use the relation Eq. (28).

Multiplying the factor

$$\frac{x(J_x,\psi_x,J_L,\phi_L)}{2\pi\sqrt{\beta_x}}\exp\left(-jq'\psi_x-j(m'-m)\phi_L\right) \tag{39}$$

by Eq. (37), before integrating the result over ϕ_L, J_x, ψ_x, J_y, ψ_y, and summing it over m', we derive

$$Dp_{q',m}(J_L)$$
$$=\sum_{m'}\int_{-\pi}^{\pi}d\phi_L\int_0^{\infty}dJ_x\int_{-\pi}^{\pi}d\psi_x\frac{x(J_x,\psi_x,J_L,\phi_L)}{2\pi\sqrt{\beta_x}}\exp\left(-jq'\psi_x-j(m'-m)\phi_L\right)$$
$$\times j\frac{e^2N_b\beta_s^2\beta_x(s)\sqrt{J_x}(\exp\left(j(\phi_x(s)-Q_x\theta)\right)\delta_{q',-1}-\exp\left(-j(\phi_x(s)-Q_x\theta)\right)\delta_{q',1})\exp\left(j\frac{2\pi\mu n}{M}\right)}{2\sqrt{2p_s}\pi R\left[\nu-m'\nu_L(J_x,J_L)-q'\nu_x(J_x,J_L)\right]}$$

$$\times \sum_{n'=0}^{M-1} \sum_{p=-\infty}^{\infty} \tilde{D}\left(\nu + p - \frac{Q_x \xi_x}{\eta}\right) \exp\left(-j\frac{2\pi\mu n'}{M} + jp\frac{2\pi(n'-n)}{M}\right) Z_T(\omega_0(\nu+p))$$
$$\times J_{m'}\left[\left(\frac{(\nu+p)\omega_{\mathrm{RF}}}{h} - \frac{Q_x\xi_x\omega_{\mathrm{RF}}}{h\eta}\right)\left(\frac{2J_L|\eta|}{cp_s\beta_s\nu_{s0}\omega_0}\right)^{1/2}\right] \frac{\partial F_0(J_x)}{\partial J_x} G_0(J_L). \tag{40}$$

Then, by substituting Eqs. (18) and (27) into Eq. (40), Eq. (40) is rewritten as

$$\begin{aligned}
&Dp_{q',m'}(J_L) \\
&= \sum_{q,m} \int_0^{\infty} dJ_x \frac{je^2 N_b \beta_s^2 \beta_x(s) J_x(\delta_{q',-1} - \delta_{q',1}) \exp\left(j\frac{2\pi\mu n}{M}\right)}{2p_s R\left[\nu - m'\nu_L(J_x,J_L) - q'\nu_x(J_x,J_L)\right]} \\
&\quad \times \sum_{n'=0}^{M-1} \sum_{p=-\infty}^{\infty} \int_0^{\infty} dJ_L' Dp_{q,m}(J_L') \exp\left(-j\frac{2\pi\mu n'}{M} + jp\frac{2\pi(n'-n)}{M}\right) Z_T(\omega_0(\nu+p)) \\
&\quad \times \frac{\partial F_0(J_x)}{\partial J_x} G_0(J_L) J_m^*\left[(\nu + p - \frac{Q_x\xi_x}{\eta})\frac{\omega_{\mathrm{RF}}}{h}\left(\frac{2J_L'|\eta|}{cp_s\beta_s\nu_{s0}\omega_0}\right)^{1/2}\right] \\
&\quad \times J_{m'}\left[(\nu + p - \frac{Q_x\xi_x}{\eta})\frac{\omega_{\mathrm{RF}}}{h}\left(\frac{2J_L|\eta|}{cp_s\beta_s\nu_{s0}\omega_0}\right)^{1/2}\right].
\end{aligned} \tag{41}$$

Here, let us introduce the function $\mathcal{D}_m$ as

$$\mathcal{D}_m(J_L) = Dp_{1,m}(J_L) + Dp_{-1,m}(J_L). \tag{42}$$

When we retain only the diagonal terms, Eq. (41) is simplified by using the function $\mathcal{D}_m$ as

$$\begin{aligned}
&\mathcal{D}_m(J_L) \\
&= -\frac{je^2 N_b M \beta_s^2 \beta_x(s) G_0(J_L)}{2p_s R} \\
&\quad \times \int_0^{\infty} dJ_x \left[\frac{1}{[\nu - m\nu_L(J_x,J_L) - \nu_x(J_x,J_L)]} - \frac{1}{[\nu - m\nu_L(J_x,J_L) + \nu_x(J_x,J_L)]}\right] \\
&\quad \times J_x \frac{\partial F_0(J_x)}{\partial J_x} \sum_{p=-\infty}^{\infty} Z_T(\omega_0(\nu+\mu+pM)) J_m\left[\left(\nu + \mu + pM - \frac{Q_x\xi_x}{\eta}\right)\left(\frac{2J_L\omega_0|\eta|}{cp_s\beta_s\nu_{s0}}\right)^{1/2}\right] \\
&\quad \times \int_0^{\infty} dJ_L' \mathcal{D}_m(J_L') J_m^*\left[\left(\nu + \mu + pM - \frac{Q_x\xi_x}{\eta}\right)\left(\frac{2J_L'\omega_0|\eta|}{cp_s\beta_s\nu_{s0}}\right)^{1/2}\right].
\end{aligned} \tag{43}$$

If we choose the functions $\mathcal{D}_m(J_L)$, $G_0(J_L)$, and $F_0(J_L)$ as

$$\mathcal{D}_m(J_L) = B_m\delta(J_L - J_{L0}), \tag{44}$$
$$G_0(J_L) = \frac{1}{2\pi}\delta(J_L - J_{L0}), \tag{45}$$
$$F_0(J_x) = \frac{1}{2\pi J_{x0}} \exp\left(-\frac{J_x}{J_{x0}}\right), \tag{46}$$

where

$$J_{x0} = \frac{\beta_s E_s \epsilon_{x,\mathrm{rms}}}{c}, \tag{47}$$

and $\epsilon_{x,\mathrm{rms}}$ is the root mean square (rms) emittance of the beam, and expand Eq. (43) around small J_x before integrating Eq. (43) over J_x, we finally obtain the dispersion relation as

$$1 \simeq -\frac{je^2 N_b M \pi \beta_s^2 \langle \beta_x(s) \rangle \left[1 + \frac{(\nu - m\nu_{L0} - \nu_{X0})}{\left(m\frac{d\nu_L}{dJ_x} + \frac{d\nu_x}{dJ_x}\right)J_{x0}} \exp\left(- \frac{(\nu - m\nu_{L0} - \nu_{X0})}{\left(m\frac{d\nu_L}{dJ_x} + \frac{d\nu_x}{dJ_x}\right)J_{x0}} \right) \Gamma\left[0, - \frac{(\nu - m\nu_{L0} - \nu_{X0})}{\left(m\frac{d\nu_L}{dJ_x} + \frac{d\nu_x}{dJ_x}\right)J_{x0}} \right] \right]}{8\pi^3 J_{x0} p_s R \left(m\frac{d\nu_L}{dJ_x} + \frac{d\nu_x}{dJ_x} \right)}$$
$$\times \sum_{p=-\infty}^{\infty} \left| J_m \left[\left(\nu + \mu + pM - \frac{Q_x \xi_x}{\eta} \right) \left(\frac{2\omega_0 J_{L0} |\eta|}{c p_s \beta_s \nu_{s0}} \right)^{1/2} \right] \right|^2 Z_T \left(\omega_0 (\Re[\nu] + \mu + pM) \right), \tag{48}$$

where

$$\nu_{L0} = \nu_{s0} + \left. \frac{dY'_{\mathrm{coh},0}(J_L)}{dJ_L} \right|_{J_L = J_{L0}}, \tag{49}$$

$$\nu_{X0} = Q_x + \frac{\langle \beta_x(s) \rangle}{p_s} Y'_{\mathrm{coh},2}(J_{L0}), \tag{50}$$

$$m\frac{d\nu_L}{dJ_x} + \frac{d\nu_x}{dJ_x} \simeq m \left. \frac{dY'_{\mathrm{coh},2}(J_L)}{dJ_L} \right|_{J_L = J_{L0}} \frac{\langle \beta_x(s) \rangle}{p_s} + 3 \left\langle \beta_x^2(s) \right\rangle Y'_{\mathrm{coh},4}(J_{L0}), \tag{51}$$

ν_{L0} and ν_{X0} are the coherent synchrotron and the betatron tunes, respectively, $\Gamma[0, z]$ is the incomplete Γ-function [27], and $\langle \cdots \rangle$ denotes the average value around the ring. Here we assume the rms beam sizes σ_x and σ_z are given as

$$\sigma_x = \left(\langle \beta_x(s) \rangle \epsilon_{x,\mathrm{rms}} + \left\langle D^2(s) \right\rangle \left(\frac{\Delta p}{p} \right)^2 \right)^{1/2} = \left(\langle \beta_x(s) \rangle \frac{c J_{x0}}{\beta_s E_s} + \left\langle D^2(s) \right\rangle \frac{2 J_{L0} \nu_{s0} \omega_0}{E_s \beta_s^2 |\eta|} \right)^{1/2}, \tag{52}$$

$$\sigma_z = \frac{c}{\omega_0} \left(\frac{2 J_{L0} |\eta| \omega_0}{E_s \nu_{s0}} \right)^{1/2}, \tag{53}$$

considering Eqs. (14), (47), (B17), (B18), and (B32). For reference, Fig. 1 illustrates typical behavior of the functions $dY'_{\mathrm{coh},0}(J_{L0})/dJ_{L0}$, $Y'_{\mathrm{coh},2}(J_{L0})$, $dY'_{\mathrm{coh},2}(J_{L0})/dJ_{L0}$, and $Y'_{\mathrm{coh},4}(J_{L0})$ in Eq. (48), which are calculated by using the beam parameters at the ramping time 15 ms in the RCS (refer to Sect. 3).

The beam growth rate and the coherent tune affected by the wake force, which are given by the real parts of $j\omega_0\nu$ and of ν, respectively, are solved by Eq. (48) as a function of nominal tune Q_x. The differences among Q_x, ν_{X0}, and $\Re[\nu]$ are tiny ($\lesssim 0.01$) in a practical situation.

2.2. *The Sacherer formula*

Here, we reproduce the classical Sacherer formula [18,19,23], where the space charge effect on the beam oscillations is neglected. In this case, the J_x and J_L dependence of the tunes ν_L and ν_x vanishes.

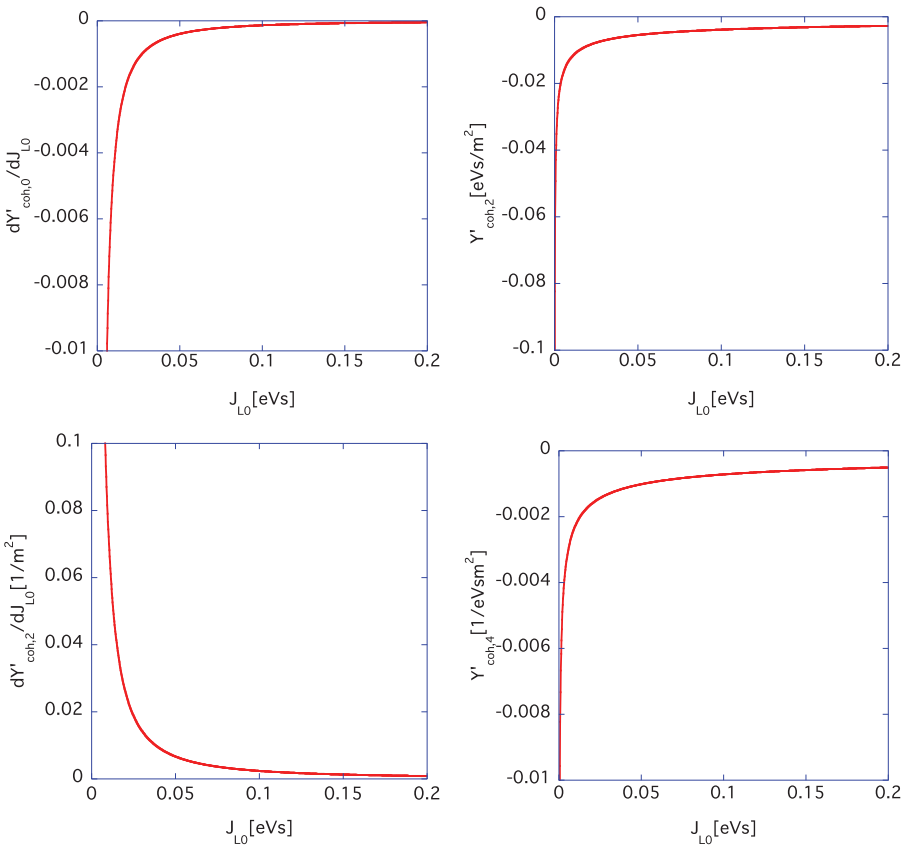

Fig. 1. Typical behavior of the functions $dY'_{\mathrm{coh},0}(J_{L0})/dJ_{L0}$ (left top), $Y'_{\mathrm{coh},2}(J_{L0})$ (right top), $dY'_{\mathrm{coh},2}(J_{L0})/dJ_{L0}$ (left bottom), and $Y'_{\mathrm{coh},4}(J_{L0})$ (right bottom) calculated by using the beam parameters at the ramping time 15 ms in the RCS.

If we confine ourselves to the case, the J_x-integration in Eq. (43) can be performed for the distribution Eq. (46). Consequently, Eq. (43) is simplified as

$$\begin{aligned}\mathcal{D}_m(J_L) = &\frac{je^2 N_b M \beta_x(s) G_0(J_L)}{4\pi p_s R}\left(\frac{1}{\nu - m\nu_{s0} - Q_x} - \frac{1}{\nu - m\nu_{s0} + Q_x}\right)\\ &\times \sum_{p=-\infty}^{\infty} Z_T(\omega_0(\nu+\mu+pM))J_m\left[\left(\nu+\mu+pM-\frac{Q_x\xi_x}{\eta}\right)\left(\frac{2J_L\omega_0|\eta|}{cp_s\nu_{s0}}\right)^{1/2}\right]\\ &\times \int_0^{\infty} dJ'_L \mathcal{D}_m(J'_L)J^*_m\left[\left(\nu+\mu+pM-\frac{Q_x\xi_x}{\eta}\right)\left(\frac{2J'_L\omega_0|\eta|}{cp_s\nu_{s0}}\right)^{1/2}\right],\end{aligned} \tag{54}$$

for an ultra-relativistic beam ($\beta_s = 1$). Here, following the conventional manner, let us replace the action-variable J_L with the amplitude-variable r_s:

$$r_s = \frac{1}{\omega_0}\left(\frac{2J_L\omega_0|\eta|}{cp_s\nu_{s0}}\right)^{1/2}, \tag{55}$$

and assume the unperturbed distribution function $G_0(J_L(r_s))$ as

$$G_0(J_L(r_s)) = \frac{|\eta|}{\pi\omega_0 cp_s\tau_{0s}^2\nu_{s0}}\Theta(\tau_{0s} - r_s), \tag{56}$$

where $\Theta(x)$ is the step function and τ_{s0} denotes the half-bunch length. Accordingly, Eq. (54) is rewritten as

$$\mathcal{D}_m(J_L(r_s)) = \frac{jce^2N_bM}{4\pi^2E_sQ_x\tau_{0s}^2}\Theta(\tau_{0s}-r_s)\left(\frac{1}{\nu-m\nu_{s0}-Q_x}-\frac{1}{\nu-m\nu_{s0}+Q_x}\right)$$
$$\times\sum_{p=-\infty}^{\infty}Z_T(\omega_0(\nu+\mu+pM))J_m\left[\omega_0\left(\nu+\mu+pM-\frac{Q_x\xi_x}{\eta}\right)r_s\right]$$
$$\times\int_0^{\infty}dr_s'r_s'\mathcal{D}_m(J_L'(r_s'))J_m^*\left[\omega_0\left(\nu+\mu+pM-\frac{Q_x\xi_x}{\eta}\right)r_s'\right], \tag{57}$$

where $\beta_x(s)$ is replaced by R/Q_x.

Let us expand the function $\mathcal{D}_m(J_L(r_s))$ using a complete set of orthogonal functions $f_k^{(m)}(r_s)$ as

$$\mathcal{D}_m(J_L(r_s)) = \tilde{W}(r_s)\sum_{k=0}^{\infty}a_k^{(m)}f_k^{(m)}(r_s) \equiv \sum_{k=0}^{\infty}a_k^{(m)}g_{m,k}(r_s), \tag{58}$$

where k is the radial mode and $\tilde{W}(r_s)$ is the weight function. The functions $f_k^{(m)}(r)$ and $g_{m,k}(r)$ satisfy the orthogonality relationship

$$\int_0^{\infty}\tilde{W}(r_s)f_k^{(m)}(r_s)f_l^{(m)}(r_s)r_s\,dr_s = \delta_{kl}, \tag{59}$$

$$\int_0^{\infty}\frac{g_{m,k}(r_s)g_{m,l}(r_s)}{\tilde{W}(r_s)}r_s\,dr_s = \delta_{kl}, \tag{60}$$

respectively. Here, the weight function $\tilde{W}(r_s)$ is defined as

$$\tilde{W}(r_s) = C\frac{\eta N_b}{\pi\tau_{0s}^2\omega_0\nu_{s0}}\Theta(\tau_{0s}-r_s), \tag{61}$$

where C is a normalization constant. Accordingly, the functions $f_k^{(m)}(r_s)$ or $g_{m,l}(r_s)$ can be revealed as

$$f_k^{(m)}(r_s) = \left(\frac{2}{\tilde{W}}\right)^{1/2}\frac{J_m(\frac{\mu_{mk}r_s}{\tau_{0s}})}{\tau_{0s}J_{m+1}(\mu_{mk})}, \quad \text{for } r_s < \tau_{0s}, \tag{62}$$

$$g_{m,l}(r_s) = \left(2\tilde{W}(r_s)\right)^{1/2}\frac{J_m(\frac{\mu_{ml}r_s}{\tau_{0s}})}{\tau_{0s}J_{m+1}(\mu_{ml})} = \left(\frac{2C\eta RN_b}{\pi c\nu_{s0}\tau_{0s}^2}\right)^{1/2}\frac{J_m(\frac{\mu_{ml}r_s}{\tau_{0s}})}{\tau_{0s}J_{m+1}(\mu_{ml})}(1-\Theta(r_s-\tau_{0s})), \tag{63}$$

where μ_{mk} is the kth zero of $J_m(x)$.

Let us introduce the particle distribution function $\rho_{m,l}(\tau)$ with head-tail mode m and radial mode l in real space as

$$\rho_{m,l}(\tau) = -\int_{-\infty}^{\infty}g_{m,l}(r_s)\exp(-jm\phi_L)\,\omega_{\mathrm{RF}}\frac{dW}{E_s} \equiv \int_{-\infty}^{\infty}g_{m,l}(r_s)\exp(-jm\phi_L)\,d\delta, \tag{64}$$

and its Fourier transform

$$\tilde{\rho}_{m,l}(k) = \int_{-\infty}^{\infty}\frac{d\tau}{2\pi}\exp(jk\tau)\,\rho_{m,l}(\tau), \tag{65}$$

where $\tau = \phi_{cp}/\omega_{RF}$ and W is the momentum conjugate to ϕ_{cp} (see Eq. (B17)).

Substituting Eq. (64) into Eq. (65), Eq. (65) is written as

$$\tilde{\rho}_{m,l}(k) = \int_0^\infty g_{m,l}(r)\frac{\omega_0 v_{s0}}{\eta} j^m J_m(kr) r\, dr, \tag{66}$$

(see Eqs. (55), (B31) and (B32)) by using the relation

$$\frac{1}{2\pi}\int_0^{2\pi} d\varphi \exp\left(il\varphi - ix\cos\varphi\right) = j^{-l}J_l[x], \tag{67}$$

while its inverse transform $\rho_{m,l}(\tau)$ is given by

$$\rho_{m,l}(\tau) = \int g_{m,l}(r)\frac{\omega_0 v_{s0}}{\eta} j^m J_m(kr)\exp\left(-jk\tau\right) r\, dr\, dk, \tag{68}$$

which is expressed as

$$\rho_{m,l}(\tau) = \left(\frac{2CRN_b v_{s0}}{\pi c\eta}\right)^{1/2}\omega_0\mu_{ml}j^m\int_0^\infty dk\frac{[((-1)^m+1)\cos k\tau + ((-1)^m-1)j\sin k\tau]J_m(k\tau_{0s})}{(\mu_{ml}^2 - k^2\tau_{0s}^2)}, \tag{69}$$

for the function given by Eq. (63). Equation (66) satisfies the relationship $\tilde{\rho}^*_{m,l}(k) = (-1)^m\tilde{\rho}_{m,l}(k)$ for real $g_{m,l}(r)$ (see Eq. (91)).

By substituting Eq. (58) into Eq. (57), in combination with Eqs. (60) and (66), Eq. (57) is solved as

$$\nu_{m,l} = Q_x + m\nu_{s0} + \frac{je^2c\eta C_{m,l}}{8\pi^2 E_s Q_x C\omega_0^2\nu_{s0}} \times \frac{\sum_{p=-\infty}^{\infty} Z_T(\omega_0(\nu+\mu+Mp))h'_{m,l}\left(\omega_0\left(Q_x + m\nu_{s0} + \mu + Mp - \frac{Q_x\xi}{\eta}\right)\right)}{\sum_{p=-\infty}^{\infty} h'_{m,l}\left(\omega_0\left(Q_x + m\nu_{s0} + \mu + Mp - \frac{Q_x\xi}{\eta}\right)\right)}, \tag{70}$$

in the lowest-order approximation, where we define the constant $C_{m,l}$ and the function $h'_{m,l}(\omega)$ as

$$C_{m,l} = \int_{-\infty}^{\infty} d\tau|\rho_{m,l}(\tau)|^2 = 2\pi\int_{-\infty}^{\infty} d\omega|\tilde{\rho}_{m,l}(\omega)|^2, \tag{71}$$

$$h'_{m,l}(\omega) \equiv |\tilde{\rho}_{m,l}(\omega)|^2, \tag{72}$$

respectively. In Eq. (70), the ω-integration is approximated by the summation of p.

The constants C and C_{ml} are determined as follows. If we impose the condition $\rho_{m,l}(\pm\tau_{0s}) = 0$ on the distribution function, the function $\rho_{m,l}(\tau)$ should be written as

$$\rho_{m,l}(\tau) = \sum_{p=1,3,5,\ldots} D_p\cos\frac{\pi p}{2\tau_{0s}}\tau + \sum_{p=2,4,6,\ldots} E_p\sin\frac{\pi p}{2\tau_{0s}}\tau, \tag{73}$$

where D_p and E_p are expansion coefficients. By equating Eq. (69) to Eq. (73), they are expressed as

$$D_p = -\frac{p\pi\omega_0\mu_{ml}}{\tau_{0s}^4}\left(\frac{2CRN_b\nu_{s0}}{\pi c\eta}\right)^{1/2}(-1)^{m/2}(-1)^{(p+1)/2}\Re\left[\int_{-\infty}^{\infty}dk\frac{J_m(k\tau_{0s})\exp(jk\tau_{0s})}{(k^2-\frac{\mu_{ml}^2}{\tau_{0s}^2})(k^2-(\frac{\pi p}{2\tau_{0s}})^2)}\right], \quad \text{for } m=0,2,4,\ldots, \tag{74}$$

$$E_p = -\frac{p\pi\omega_0\mu_{ml}}{\tau_{0s}^4}\left(\frac{2CRN_b\nu_{s0}}{\pi c\eta}\right)^{1/2}(-1)^{(m-1)/2}(-1)^{p/2}\Im\left[\int_{-\infty}^{\infty}dk\frac{J_m(k\tau_{0s})\exp(jk\tau_{0s})}{(k^2-\frac{\mu_{ml}^2}{\tau_{0s}^2})(k^2-(\frac{\pi p}{2\tau_{0s}})^2)}\right], \quad \text{for } m=1,3,5,\ldots, \tag{75}$$

where we use

$$\int_{-\tau_{0s}}^{\tau_{0s}}\cos k\tau\cos\frac{\pi p\tau}{2\tau_{0s}}d\tau = \frac{(-1)^{(p+1)/2}p\pi}{\tau_{0s}\left(k^2-(\frac{\pi p}{2\tau_{0s}})^2\right)}\cos k\tau_{0s}, \quad \text{for odd } p, \tag{76}$$

$$\int_{-\tau_{0s}}^{\tau_{0s}}\sin k\tau\sin\frac{\pi p\tau}{2\tau_{0s}}d\tau = \frac{(-1)^{p/2}p\pi}{\tau_{0s}\left(k^2-(\frac{\pi p}{2\tau_{0s}})^2\right)}\sin k\tau_{0s}, \quad \text{for even } p, \tag{77}$$

$$J_m(-x) = (-1)^m J_m(x). \tag{78}$$

By picking up the residues, the k-integration in Eqs. (74) and (75) is performed. As a result, we obtain

$$D_p = \frac{\omega_0}{\tau_{0s}}\left(\frac{\pi CRN_b\nu_{s0}}{c\eta}\right)^{1/2}(-1)^{m/2}\frac{2\sqrt{2}\mu_{ml}J_m(\frac{\pi p}{2})}{\left(\mu_{ml}^2-(\frac{\pi p}{2})^2\right)}, \quad \text{for even } m, \tag{79}$$

$$E_p = \frac{\omega_0}{\tau_{0s}}\left(\frac{\pi CRN_b\nu_{s0}}{c\eta}\right)^{1/2}(-1)^{(m-1)/2}\frac{2\sqrt{2}\mu_{ml}J_m(\frac{\pi p}{2})}{\left(\mu_{ml}^2-(\frac{\pi p}{2})^2\right)}, \quad \text{for odd } m. \tag{80}$$

Finally, $\rho_{m,l}(\tau)$ is summarized as

$$\rho_{m,l}(\tau) = \sum_p A_{lp}^m b_p(\tau), \tag{81}$$

$$b_p(\tau) = \begin{cases}\cos\frac{\pi p\tau}{2\tau_{0s}}, & \text{for } p=1,3,5,\ldots,\\ \sin\frac{\pi p\tau}{2\tau_{0s}}, & \text{for } p=2,4,6,\ldots,\end{cases} \tag{82}$$

$$A_{lp}^m = \frac{\omega_0}{\tau_{0s}}\left(\frac{\pi CRN_b\nu_{s0}}{c\eta}\right)^{1/2}P_{m,p,l}\begin{cases}(-1)^{m/2}, & \text{for } m=0,2,4,\ldots,\\ (-1)^{(m-1)/2}, & \text{for } m=1,3,5,\ldots,\end{cases} \tag{83}$$

$$P_{m,p,l} = \frac{2\sqrt{2}\mu_{ml}J_m(\frac{\pi p}{2})}{(\mu_{ml}^2-\frac{\pi^2p^2}{4})}, \tag{84}$$

where p runs $1,3,5,\ldots$ for $m=0,2,4,\ldots$, and p runs $2,4,6,\ldots$ for $m=1,3,5,\ldots$.

Here, let us focus on the lowest-order term for the radial mode $l = 1$. The factor

$$\frac{8\mu_{m1}^2 J_m^2(\frac{\pi(m+1)}{2})}{(\mu_{m,1}^2 - \frac{\pi^2(m+1)^2}{4})^2}, \tag{85}$$

which appears in Eq. (70), dominates for the component $m + 1 = p$. Then, the function $\rho_{m,l=1}(\tau)$, its Fourier transform $\tilde{\rho}_{m,l=1}(\omega)$, and the factor $P_{m,p=m+1,l=1}$ are approximated as

$$\rho_{m,l=1}(\tau) = \begin{cases} (-1)^{\frac{m}{2}} \cos\frac{\pi(m+1)\tau}{2\tau_{0s}}, & \text{for } m = 0, 2, 4, \ldots, \\ (-1)^{\frac{m-1}{2}} \sin\frac{\pi(m+1)\tau}{2\tau_{0s}}, & \text{for } m = 1, 3, 5, \ldots, \end{cases} \tag{86}$$

$$\tilde{\rho}_{m,l=1}(\omega) = \begin{cases} (-1)^{m/2} \int_{-\tau_{0s}}^{\tau_{0s}} \frac{d\tau}{2\pi} \exp(j\omega\tau) \cos\frac{\pi(m+1)\tau}{2\tau_{0s}} = \frac{2\tau_{0s}(1+m)\cos\omega\tau_{0s}}{\pi^2\left[(1+m)^2 - \frac{4\omega^2\tau_{0s}^2}{\pi^2}\right]}, \\ \qquad\qquad\qquad\qquad\qquad\qquad\qquad\qquad \text{for } m = 0, 2, 4, \ldots, \\ (-1)^{(m-1)/2} \int_{-\tau_{0s}}^{\tau_{0s}} \frac{d\tau}{2\pi} \exp(j\omega\tau) \sin\frac{\pi(m+1)\tau}{2\tau_{0s}} = \frac{j(1+m)2\tau_{0s}\sin\omega\tau_{0s}}{\pi^2\left[(1+m)^2 - \frac{4\omega^2\tau_{0s}^2}{\pi^2}\right]}, \\ \qquad\qquad\qquad\qquad\qquad\qquad\qquad\qquad \text{for } m = 1, 3, 5, \ldots, \end{cases} \tag{87}$$

and

$$P_{m,p=m+1,l=1} = \frac{2\sqrt{2}\mu_{m,1}J_m(\frac{\pi(m+1)}{2})}{(\mu_{m,1}^2 - \frac{\pi^2(m+1)^2}{4})} \simeq \frac{16(3+2m)}{(5+4m)\pi^2\sqrt{m+1}} \sim \frac{1}{\sqrt{m+1}}, \tag{88}$$

respectively. Substituting Eq. (86) into Eq. (71), we finally obtain

$$C_{m,l} = \tau_{0s}. \tag{89}$$

The constant C is determined by the condition $A^m_{l=1,p=m+1} = 1$. As a result, it is calculated as

$$C = \frac{\eta c(m+1)\tau_{0s}^2}{\omega_0^2 \nu_{s0}\pi R N_b}. \tag{90}$$

Accordingly, the function $g_{m,l}(r_s)$ is described as

$$g_{m,l}(r_s) = \frac{\sqrt{2(m+1)}|\eta| J_m(\frac{\mu_{ml} r_s}{\tau_{0s}})}{\pi\omega_0\nu_{s0}\tau_{0s}J_{m+1}(\mu_{ml})}(1 - \Theta(r_s - \tau_{0s})), \tag{91}$$

owing to Eqs. (63) and (90).

By summarizing all these results (by substituting Eqs. (89) and (90) into Eq. (70), and by calculating Eq. (72) with Eq. (87)), we finally derive the conventional Sacherer formula:

$$\tau_m^{-1} = -\frac{cI_c}{4\pi Q_x(m+1)E_s/e} \sum_{p=-\infty}^{\infty} \Re[Z_T(\omega_p')]F_m'(\omega_p' - \omega_\xi), \tag{92}$$

where τ_m^{-1} is the growth rate,

$$F_m'(\omega) = \frac{h_m'(\omega)}{B_f' \sum_{p=-\infty}^{\infty} h_m'(\omega_p' - \omega_\xi)}, \tag{93}$$

$$h'_m(\omega) = \frac{(2\tau_{0s})^2}{2\pi^4}(m+1)^2\frac{[1+(-1)^m\cos(\omega 2\tau_{0s})]}{\left[(\frac{\omega 2\tau_{0s}}{\pi})^2-(m+1)^2\right]^2}, \tag{94}$$

$$\omega'_p = \omega_0(Q_x + m\nu_{s0} + \mu + Mp), \tag{95}$$

$$\omega_\xi = \omega_0\frac{Q_x\xi}{\eta}, \tag{96}$$

$$I_c = \frac{eMN_b}{T_0}, \tag{97}$$

$$B'_f = \frac{M2\tau_{0s}c}{2\pi R}. \tag{98}$$

In this paper's calculations, the factor B'_f is approximated by the typical bunching factor B_f defined by the average current divided by the peak current (see Eq. (101)).

3. RCS parameters and the beam growth rate estimated by the Sacherer formula

At the RCS, the bunched beams are formed by accumulating the injection beam from the LINAC with a painting scheme [28,29]. They are accelerated from 400 MeV to 3 GeV over 20 ms. Figure 2 shows the typical patterns of the acceleration voltage $V_{\rm rf}$ (red), and of the synchronous phase φ_s (blue) in that period. Table 1 shows typical machine and beam parameters for the RCS, which were used in this paper's calculations. The average chamber radius a around the ring is determined to be 145 mm, in order that the coherent betatron tune shift reproduces the measured date for a 400 MeV beam.

Eight kickers are installed in the RCS. The real and the imaginary parts of the horizontal impedance $Z_T(\omega)$ for one kicker are shown in the left and the middle panels of Fig. 3, respectively. The red and blue lines show the impedances at $\beta_s = 0.7$ and $\beta_s = 1$, respectively. The impedance is roughly proportional to the Lorentz-β [15]. The corresponding wake function $W_T(\omega_0 t)$ calculated by Eq. (17) is denoted by the same color in the right-hand figure. The reflection wave excited at the end of the power cable of the kicker creates the spike structure of the kicker impedance.

As shown in the left and middle panels, the impedance is very large indeed. We have demonstrated that the RCS is a kicker-impedance-dominated machine by stabilizing unstable beams by temporarily

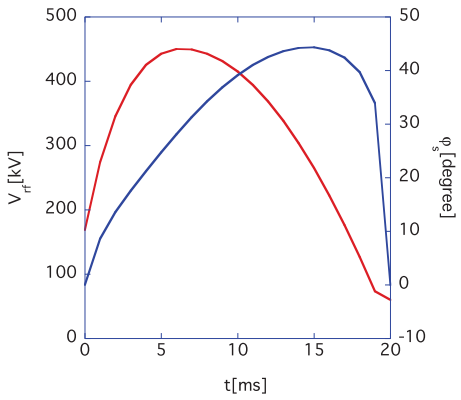

Fig. 2. Typical pattern of the acceleration voltage $V_{\rm rf}$ (red), and the synchronous phase φ_s (blue) during the ramping time.

Table 1. Typical parameter list

T (kinetic energy, GeV)	0.4	3
f_0 (revolution frequency, MHz)	0.61	0.84
η (slippage factor)	-0.478	-0.047
I_c (average current, A)	8.1	11.2
ν_{s0} (synchrotron tune)	0.0053	0.0005
$\langle\beta_x(s)\rangle$ (m)	11.6	
$\langle\beta_x^2(s)\rangle$ (m^2)	172.3	
$\langle D^2(s)\rangle$ (m)^2	3.46	
$\epsilon_{x,\mathrm{rms}}$ (mmrad)	$100/6\beta_s\gamma_s$	
J_{L0} (eV · s)	0.1645	

(Circumference $C = 348.333$ m, harmonic number $h = 2$, repetition rate = 25 Hz, particles per bunch $N_b = 4.15 \times 10^{13}$, and the average chamber radius $a = 145$ mm).
Here, $\beta_x(s)$ and $D(s)$ are the β-function and the dispersion function, respectively; $\epsilon_{x,\mathrm{rms}}$ and J_{L0} are the root mean square (rms) horizontal and the longitudinal emittances, respectively; $\langle\cdots\rangle$ denotes the average value around the ring; and β_s and γ_s are the Lorentz-β and Lorentz-γ on the designed particle.

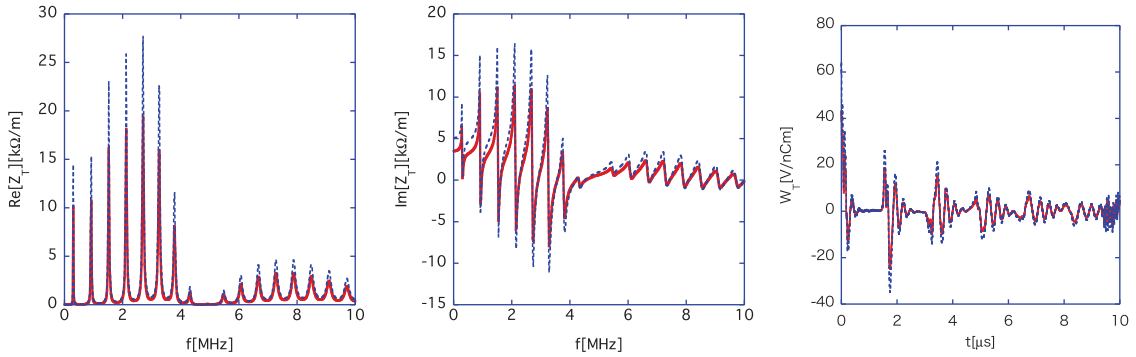

Fig. 3. Dependence of the horizontal kicker impedance $Z_T(\omega)$ (left/middle) and of the wake function $W_T(\omega_0 t)$ (right) on the Lorentz-β. The red and blue lines show the results at $\beta_s = 0.7$ and $\beta_s = 1$, respectively. The wave propagation speeds in the kicker magnet and in the power cable are about $0.02 \times c$ and $0.57 \times c$, respectively. The magnet length and the cable length are 705 mm and 130 m, respectively.

reducing the impedance [12,13]. For simplicity, we assume in this paper that the only source of impedance in the RCS is kicker impedance.

Mostly (except the discussion about chromaticity dependence of beam growth rates shown in Figs. 16 and 17), let us consider a case in which the chromaticity ξQ_x is activated by a DC-power supply at the injection energy. In this case the chromaticity approaches the natural chromaticity ($\xi Q_x = -10.3$) [30] as the beam energy is increased, as shown in Fig. 4.

We have observed beam instabilities at the J-PARC RCS, where the chromaticity was fully corrected only at the injection energy. The blue line of Fig. 5 shows an example of the results of the horizontal beam position for a 750 kW equivalent beam (3.10×10^{13} particles per bunch). For reference, the green line shows the results where only one bucket among the two is filled with one bunched beam. Since no instability occurs on the green line, we have judged that the instabilities on the blue line are the coupled-bunch instabilities.

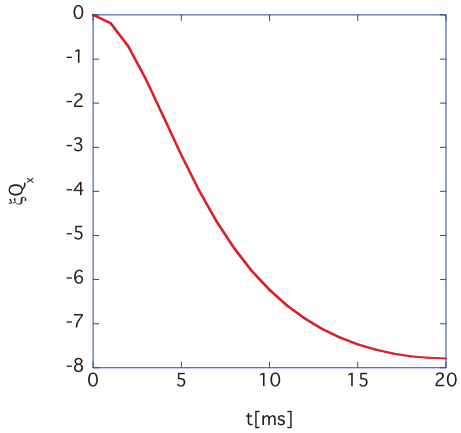

Fig. 4. Calculated chromaticity ξQ_x change during the ramping time.

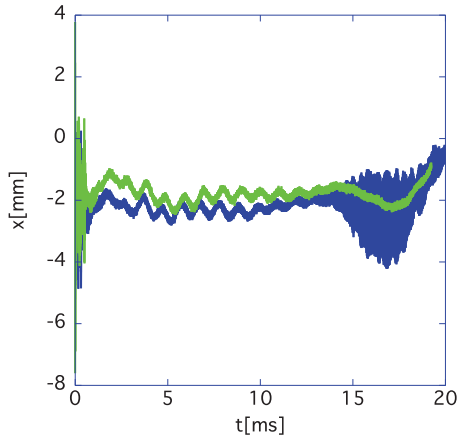

Fig. 5. Measured horizontal beam positions for the case of 3.10×10^{13} particles per bunch and $Q_x = 6.45$. The blue line shows the results where two buckets are perfectly filled with two bunches, and the green line shows the results where only one bucket among the two is filled with one bunch. The momentum spread of the injection beam from LINAC is 0.18%.

Figure 6 shows the measured results for a 1 MW equivalent beam (4.15×10^{13} particles per bunch), where the chromaticity was fully corrected only at the injection energy. Both results for 750 kW equivalent and 1 MW equivalent beams have demonstrated that the beam is stable at low energies, while they tend to be unstable at high energies.

Here, let us investigate whether the conventional Sacherer formula Eq. (92) can explain the measured beam behavior. From now on, we assume that the maximum number of the head-tail mode m is 5, and that the coupled mode μ runs from 0 to 1. Figure 7 shows the theoretical results for the case. The results predict that the beam is unstable at low energies, while it is stable at high energies. These results suggest that a partial chromaticity correction at low energies should enhance the beam instability at low energies. However, these theoretical results (Fig. 7) differ significantly from the measured data (Figs. 5 and 6).

The measurement results indicate that space charge stabilizes the beam instability at low energies. Note that Eq. (92) is derived by neglecting this effect. In the next section, let us theoretically examine the space charge effect on the beam instability at the RCS.

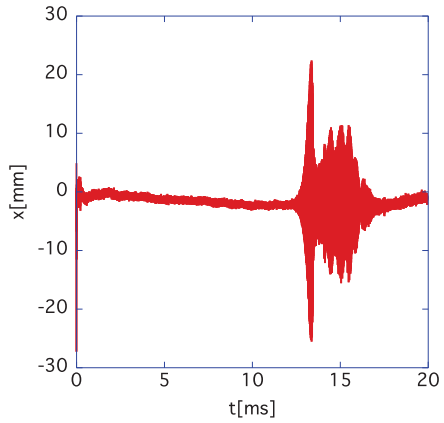

Fig. 6. Measured horizontal beam positions for the case of 4.15×10^{13} particles per bunch and $Q_x = 6.45$. The momentum spread of the injection beam is 0.18%.

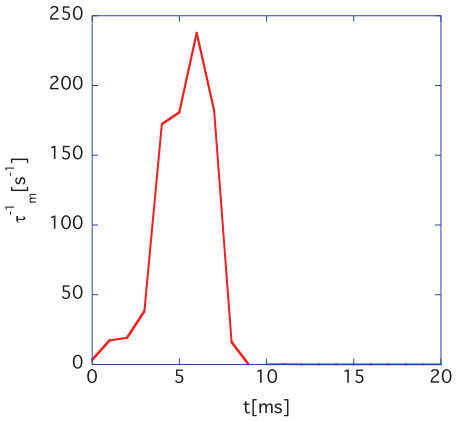

Fig. 7. The maximum beam growth rate among with different modes (m, μ) estimated by using the Sacherer formula, Eq. (92), for $Q_x = 6.45$.

4. Investigation of the beam instability at the RCS

4.1. Space charge effects on the beam growth rate

The Landau damping caused by the space charge effect appears in Eq. (51). Because this equation depends only on the longitudinal emittance J_{L0} in our model, only the longitudinal size of the beam is likely to affect the effect, significantly. However, the true space charge effect is revealed in Eq. (48) after integration with respect to J_x according to Eq. (43). In particular, the damping effect is neglected for a beam with infinitesimal transverse beam size, and Eq. (48) is sufficiently well approximated by the analytical formula

$$\nu \simeq m\nu_{L0} + \nu_{X0} + \frac{je^2 N_b M \pi c \beta_s \langle \beta_x(s) \rangle}{8\pi^3 E_s R} \times \sum_{p=-\infty}^{\infty} \mathcal{F}^m \left(J_{L0}, m\nu_{L0} + \nu_{X0} + \mu + pM - \frac{Q_x \xi_x}{\eta} \right) Z_T(\omega_0(m\nu_{L0} + \nu_{X0} + \mu + pM)), \quad (99)$$

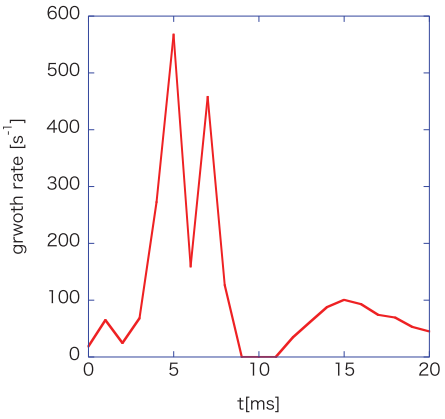

Fig. 8. The maximum beam growth rate among different modes (m, μ) estimated by Eq. (99) for $Q_x = 6.45$.

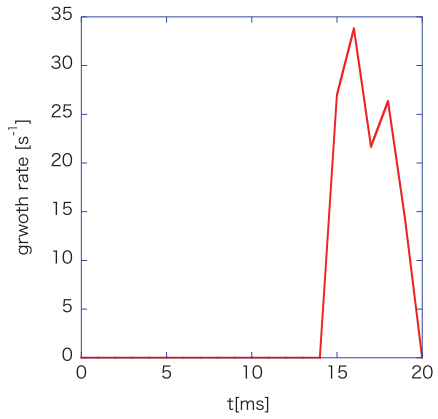

Fig. 9. The maximum beam growth rate among different modes (m, μ) estimated by solving Eq. (48) for $Q_x = 6.45$.

where

$$\mathcal{F}^m(J_{L0}, x) = \left| J_m \left[x \left(\frac{2\omega_0 J_{L0}|\eta|}{c p_s \beta_s \nu_{s0}} \right)^{1/2} \right] \right|^2 . \tag{100}$$

Figure 8 shows the maximum beam growth rate among different modes (m, μ) estimated according to Eq. (99). As in the results obtained using the conventional formula (shown in Fig. 7), these results show that the beam is unstable at low energies. However, this result successfully explains the beam instability of the measured results at high energies, which the conventional formula does not explain. To understand the beam stabilization at low energies, the Landau damping effects owing to space charge must be taken into account.

Here, let us investigate the effect more closely. First, we present the theoretical results of taking the space charge effect into account for the maximum beam growth rate by solving Eq. (48). The results are shown in Fig. 9. Comparing the results shown in Fig. 8 with the present results, we find that the beam is stabilized at low energies and that the theoretical results explain well the characteristic of the measurement ones (shown in Figs. 5 and 6). We can see a sharp rise at $t = 13$ ms only in the measured data of the 1 MW-equivalent beam (Fig. 6). The space charge damping effect seems to be drastically reduced for a beam with larger oscillation amplitudes. If this is a kind of nonlinear phenomenon, our theory, based on the linearized Vlasov equation, has a limit to explain it.

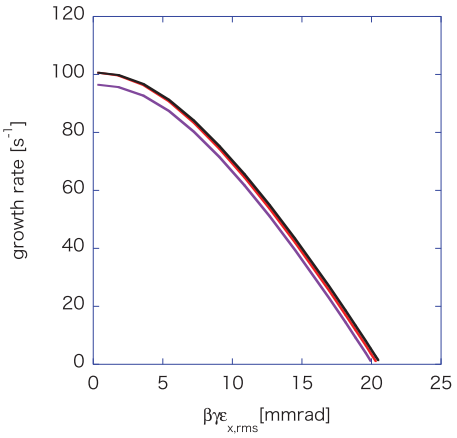

Fig. 10. Theoretical results of the transverse beam emittance $\epsilon_{x,\mathrm{rms}}$ dependence of the beam growth rate at 15 ms for $Q_x = 6.45$. The red, black, and purple lines are the beam growth rates excited by $(m = 0, \mu = 1)$, $(m = 2, \mu = 1)$, and $(m = 4, \mu = 1)$ modes, respectively.

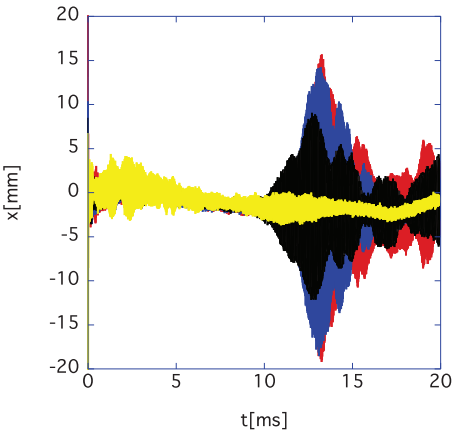

Fig. 11. Measurement results ($N_b = 4.15 \times 10^{13}$) of the horizontal beam positions for different transverse painting areas, where the chromaticity was fully corrected only at the injection energy. The red, blue, black, and yellow lines show the results for 0π (center injection), 100π, 150π, and 200π mmrad injection painting schemes, respectively, where the tune Q_x changes during the ramping time following the black line in the right panel of Fig. 14. The momentum spread of the injection beam from LINAC is 0.18%.

Figure 10 shows the theoretical results of the transverse beam emittance dependence of the beam growth rate. The red, black, and purple lines are the beam growth rates excited by $(m = 0, \mu = 1)$, $(m = 2, \mu = 1)$, and $(m = 4, \mu = 1)$ modes, respectively (the growth rate excited by the other modes is negligibly low.). As already explained, the Landau damping effect becomes ineffective for all modes, as the transverse emittance decreases. Figure 11 illustrates the measured beam positions for different transverse emittances. The red, blue, black, and yellow lines show the results for the cases that the injection painting areas are 0π (center injection), 100π, 150π, and 200π mmrad, respectively [28,29]. The emittance dependence is clearly observable in the results. As the painting area is larger at the injection period, the beam tends to be more stabilized at high energies.

Thus, we find that the Landau damping effect owing to the space charge (depending on the longitudinal beam size) is enhanced by enlarging the transverse beam size. From a phenomenological point of view, the space charge damping effect is easily activated for the lower-energy beam, as a result of the larger transverse beam emittance.

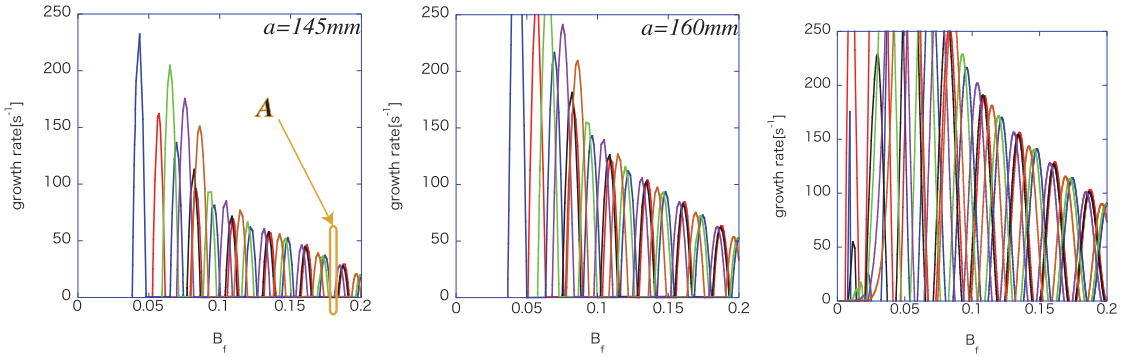

Fig. 12. Theoretical results of the beam growth rate (at 15 ms for $Q_x = 6.45$) with (left/middle) and without (right) space charge effects, dependence on the bunching factor. The red, blue, black, green, purple, and brown lines are the beam growth rates excited by $(m = 0, \mu = 1)$, $(m = 1, \mu = 1)$, $(m = 2, \mu = 1)$, $(m = 3, \mu = 1)$, $(m = 4, \mu = 1)$, and $(m = 5, \mu = 1)$ modes, respectively. The left and the middle panels show the results for the chamber radii $a = 145$ mm and $a = 160$ mm, respectively.

Now, let us closely investigate the bunching factor B_f (longitudinal beam size) dependence of the beam growth rate for different head-tail and coupled-bunch modes (m, μ). Figure 12 shows the theoretical results of the beam growth rate at 15 ms, where the bunching factor B_f is evaluated by using

$$B_f = \frac{4}{3(\pi - \phi_e - \varphi_s)} \left(\frac{2J_{L,0} h^2 |\eta| \omega_0}{E_s \beta_s^2 \nu_{s0}} \right)^{1/2}, \tag{101}$$

where ϕ_e is the solution of

$$\cos\phi_e + \phi_e \sin\varphi_s + \cos\varphi_s - (\pi - \varphi_s)\sin\varphi_s = 0, \tag{102}$$

which satisfies the condition $-\pi < \phi_e < 0$ [31]. The left and the middle panels of Fig. 12 illustrate the beam growth rates with space charge effects for the chamber radii $a = 145$ mm and $a = 160$ mm, respectively. The right panel illustrates the beam growth rate without space charge effects calculated by using Eq. (99). The red, blue, black, green, purple, and brown lines are the beam growth rates excited by $(m = 0, \mu = 1)$, $(m = 1, \mu = 1)$, $(m = 2, \mu = 1)$, $(m = 3, \mu = 1)$, $(m = 4, \mu = 1)$, and $(m = 5, \mu = 1)$ modes, respectively (the other modes do not excite the beam instabilities).

The conventional Sacherer formula (92) indicates that the beam growth rate without space charge is roughly inversely proportional to the bunching factor B_f. The left and middle panels demonstrate that the overall behavior of the beam growth rate including space charge effect is also roughly inversely proportional to the bunching factor B_f. However, the beam is ultimately stabilized in the extremely compressed beam (with the extremely small bunching factor). In this case, the Landau damping due to the space charge force absolutely stabilizes the beam instability.

The beam growth rates for the different modes (m, μ) in all panels of Fig. 12 reveal the respective comb-like structures along the bunching factor. The behavior originates from the head-tail motion of the beam, as shown in the form factor $\mathcal{F}^m(J_L, x)$ in Eq. (99). Thus, when we fix a mode, the beam growth rate for the mode follows the characteristic comb-like behavior, even in the results without space charge effect (right). However, because the growth rate patterns are overlapped for the different modes (m, μ) in the results without space charge effect, it is hard to specify the optimized point along the bunching factor from the viewpoint of beam instability. Thus, we reach the conventional

conclusion that the larger bunching factor (smaller peak current) is preferable for beam stabilization, when the space charge effect is neglected.

Contrary to the such conventional understanding, beam stabilized regions emerge along the bunching factor in the results with the space charge effects for $a = 145\,\mathrm{mm}$ (e.g., around the area A). Comparing both the results for $a = 145\,\mathrm{mm}$ (left) and for $a = 160\,\mathrm{mm}$ (middle), we find that the bandwidth of the stabilized region caused by the space charge effect significantly depends on the chamber radius a. Though the difference between the chamber radii is only 15 mm, the beam stabilization area A in the results for $a = 145\,\mathrm{mm}$ (left) disappears in the results for $a = 160\,\mathrm{mm}$ (middle). In conclusion, the smaller chamber radius is preferable in view of the beam stabilization to make maximum use of the space charge damping effect.

The existence of such a beam stabilization region, stemming from the space charge effects, along the bunching factor can be demonstrated at a low-energy proton ring like the RCS. At the RCS, the bunching factor can be changed by changing the momentum spread of the injection beam from the LINAC. We can prepare two types of injection beams: $dp/p = 0.08\%$ and $dp/p = 0.18\%$. The injection beam with the smaller momentum spread creates an accumulated beam with a smaller bunching factor. The measurement results for the beam positions and their corresponding bunching factors are illustrated in Fig. 13 with the same colors, where the number of particles per bunch is 3.10×10^{13}. It is observable that the beam can be more stabilized with the smaller bunching factor, contrary to conventional understanding. Theoretically, this stabilization is caused by the dip around the area A in Fig. 12.

4.2. The effects of tune manipulation on beam growth rate

Here, let us illustrate the tune dependence of the beam growth rate. The measurement results are shown in the left panel of Fig. 14. The tracking pattern of the tune during the acceleration period is shown in the right panel of Fig. 14 using the same color. The results represented by the red line correspond to the highest beam growth rate case. The second highest case is represented by the yellow line. The most stable case is indicated by the black line, which is sandwiched by these two unstable cases (the red and the yellow lines). Figure 15 shows the theoretical results of the beam growth rate at 15 ms, which are obtained by solving Eq. (48). The red, black, and purple lines are the beam growth rates excited by the $m = 0$, $m = 2$, and $m = 4$ modes, respectively. The solid and

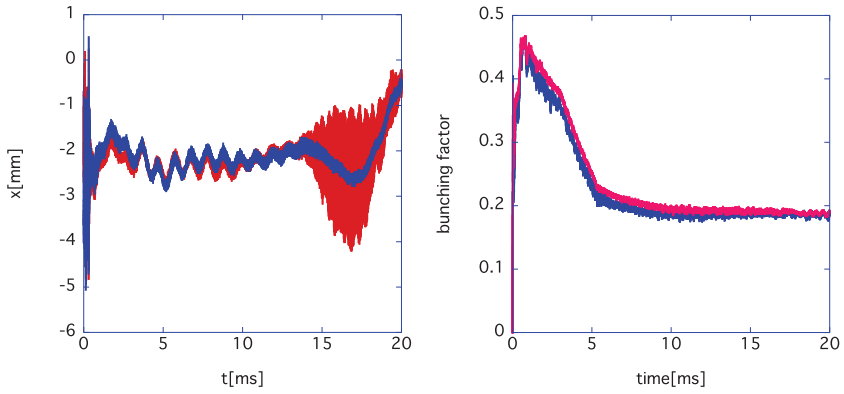

Fig. 13. Beam growth rate (for 3.10×10^{13} particles per bunch) dependence on the bunching factor, where the tune is fixed to 6.45. The chromaticity was fully corrected only at the injection energy. The left panel shows the measured beam positions for two different bunching factors. The right panel shows the measured bunching factor. The two lines with the same color in both figures denote identical situations.

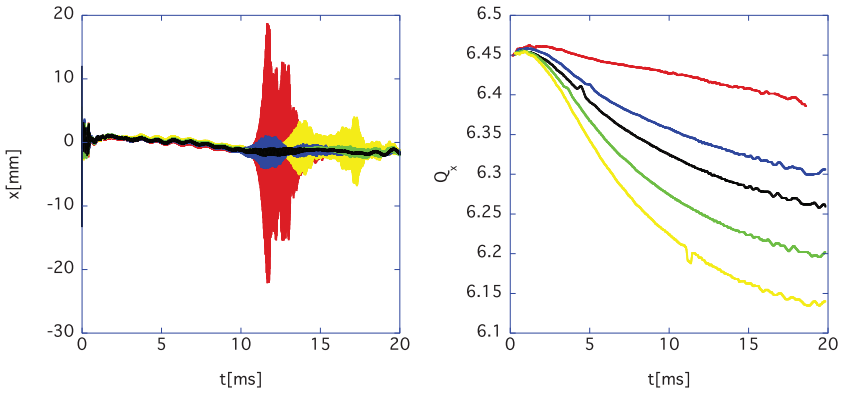

Fig. 14. The left panel shows the measured (4.15×10^{13} particles per bunch) beam positions for five different tune tracking patterns, where the chromaticity was fully corrected only at the injection energy. The right panel shows the measured tune tracking patterns under the condition that the space charge effect is negligible. The lines of matching color in each panel denote identical situations. The momentum spread of the injection beam is 0.08%.

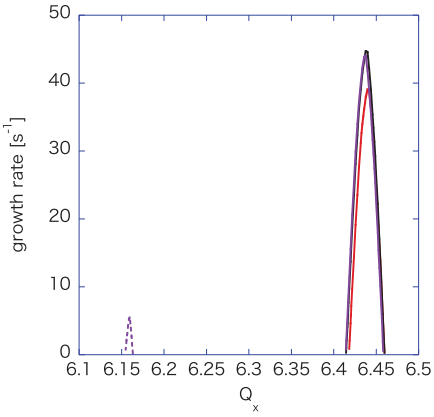

Fig. 15. Dependence of the theoretical results of the beam growth rate at 15 ms on the tune Q_x. The red, black, and purple lines are the beam growth rates excited by the $m = 0$, $m = 2$, and $m = 4$ modes, respectively. The solid and dashed lines show the $\mu = 1$ and $\mu = 0$ modes, respectively.

dashed lines show the $\mu = 1$ and $\mu = 0$ modes, respectively (the other head-tail modes do not excite the beam instabilities). The theoretical calculation explains the characteristic of the tune dependence of the beam growth rate sufficiently well, as revealed by the measured results (Fig. 14). The tune dependence of the beam growth rate originates from the spike structure of the kicker impedance (see Fig. 3).

Finally, we illustrate the chromaticity dependence of the beam growth rate. Figure 16 shows the theoretical results of the beam growth rate at 15 ms for $Q_x = 6.45$. The red, blue, black, green, purple, and brown lines are the beam growth rates excited by the $(m = 0, \mu = 1)$, $(m = 1, \mu = 1)$, $(m = 2, \mu = 1)$, $(m = 3, \mu = 1)$, $(m = 4, \mu = 1)$, and $(m = 5, \mu = 1)$ modes, respectively (the other modes do not excite the beam instabilities). We expect that the beam growth rate will be drastically suppressed, as the chromaticity correction is weakened.

The measured results are shown in Fig. 17. To clearly observe the chromaticity dependence of the beam growth rate, let us study the highest growth rate case (the tracking pattern of the tune is designated by the red line in the right panel of Fig. 14). The red, blue, and black lines in Fig. 17

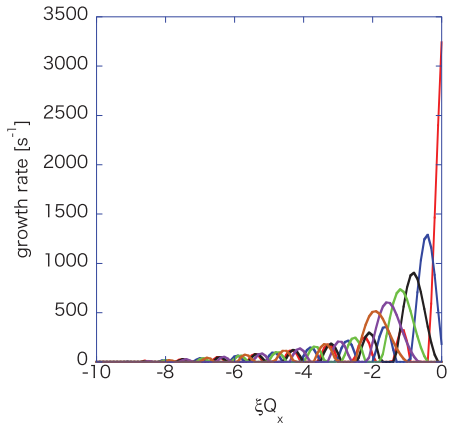

Fig. 16. Theoretical results of the beam growth rate at 15 ms dependence on the chromaticity ξQ_x for $Q_x = 6.45$. The red, blue, black, green, purple, and brown lines are the beam growth rates excited by the $(m = 0, \mu = 1)$, $(m = 1, \mu = 1)$, $(m = 2, \mu = 1)$, $(m = 3, \mu = 1)$, $(m = 4, \mu = 1)$, and $(m = 5, \mu = 1)$ modes, respectively.

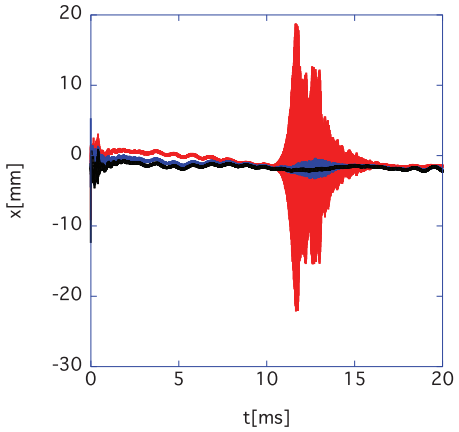

Fig. 17. Measured beam positions ($N_b = 4.15 \times 10^{13}$, $dp/p = 0.08\%$) with different chromaticity, where the tune changes, following the red line in the right panel of Fig. 14. The red, blue, and black lines show the results for which, at the injection energy only, the chromaticity was fully, half, and quarter corrected, respectively.

show, respectively, the results for which the chromaticity was fully corrected only at the injection energy by the DC-power supply, half corrected compared to the full correction, and quarter corrected in the same manner. Concretely, the chromaticity values at 15 ms are -7.46 for the red line, -8.92 for the blue line, and -9.64 for the black line. As expected, the beam is drastically suppressed by an increase in chromaticity in the negative direction.

5. Summary

The RCS in J-PARC, where kicker impedance dominates, is a special machine from an impedance viewpoint, which means that the RCS violates the impedance budget from a classical viewpoint [6,18, 19]. Nevertheless, we have successfully accelerated a 1 MW equivalent beam (4.15×10^{13} particles per bunch). The RCS is an accelerator covering the intermediate beam energy region (from 400 MeV to 3 GeV). Thus, it is pertinent to study the space charge effects on the beam instability.

The machine has some interesting characteristics: e.g., the beam can be stabilized by reducing the bunching factor (increasing the peak current) and the beam tends to be unstable when reducing the transverse beam size. The classical theory, i.e., Sacherer's theory, fails to explain these characteristics by neglecting the space charge effects.

Recently, there has been a significant development in the field of computer technologies. Numerical computer simulations are powerful tools to quantitatively estimate the beam behavior associated with space charge effects [32–34]. It may seem that a numerical simulation study is sufficient to accelerate beams from a practical viewpoint.

However, such simulations take excessive CPU time and memory for one set of fixed parameters. If we theoretically understand what conditions (parameters sets) excite beam instabilities in combination with space charge effects in advance, numerical studies are more efficiently performed by selecting the appropriate parameters sets, based on the theoretical comprehension. Consequently, we can focus on the quantitative discussion about the issues concerning beam commissioning (beam loss, beam halo, etc.). Moreover, the theoretical study is vital to understand the nature of the phenomena concerning beams in accelerators.

In this paper, we try to understand the beam instabilities associated with the space charge effects by developing a new theory. And, we have clarified the parameters (such as the transverse emittance, the bunching factor, etc.) dependence on the beam growth rate.

The space charge damping effect is significant at low energies, not only due to the smaller Lorentz-γ but also due to the larger transverse beam size. The large transverse emittance is essential to activate the Landau damping owing to the space charge effect.

It is of interest that the beam growth rate is suppressed by increasing the peak current (shortening the bunch length, or reducing the bunching factor) at the RCS. Theoretically, the beam growth rate for different modes (m, μ) follows different characteristic comb-like structures along the bunching factor. The dependence of the beam growth rate on the bunching factor originates from the head-tail motion of the beam. Thus, even in the case without the space charge effect, the beam growth rate for one fixed mode can be suppressed by increasing the peak current (shortening the bunch length, or reducing the bunching factor).

However, the beam growth rates excited by different modes (m, μ) are sufficiently overlapped along the bunching factor in the case. Finally, the theory reproduces the conventional conclusion that the maximum beam growth rate among different modes (m, μ) is reduced by increasing the bunch length (reducing the peak current or increasing the bunching factor) when the space charge effect is neglected.

On the contrary, if we take the space charge effect into consideration, the overlap of the beam growth rates for different modes (m, μ) is separated over the axis of the bunching factor, and some beam stabilization regions emerge on the axis. The optimization of bunching factor enables the beam to be stabilized, regardless of the amount of the bunching factor, in a lower-energy proton synchrotron like the RCS.

The space charge damping effect is quite sensitive to the chamber radius. Consequently, a smaller radius chamber is preferable from a beam instability point of view. As the beam energy becomes higher, the space charge damping effect becomes less effective, and the beam stabilization region diminishes along the bunching factor.

In a low-energy proton machine, such as the RCS, the violation of the impedance budget from a classical viewpoint is not vital to achieve high intensity beams. They can be realized by optimizing the machine's (beam) parameters, i.e., the bunching factor, transverse emittance, tune, chromaticity, etc.

Acknowledgements

The authors would like to thank Kazuhito Ohmi, Jie Wei, Katsunobu Oide, Yoshishige Yamazaki, Tadashi Koseki, Kazuo Hasegawa, and Michikazu Kinsho for fruitful discussions. They also would like to thank all members of the J-PARC Accelerator Technical Advisory Committee, which was led by Steve Holmes until 2009, and has been led by Thomas Roser since 2010. The authors would also like to thank all the members of the J-PARC project at JAEA/KEK.

Appendix A. A solution of the Poisson equation with cylindrical chamber

In this section, we show how to solve the Poisson equation for an axisymmetric beam that is surrounded by a perfectly conductive cylindrical chamber with radius a. The Poisson equation in the rest frame of the beam $(c\bar{t}, x, y, \bar{z})$ is described by

$$\frac{\partial^2 \bar{\Phi}}{\partial x^2} + \frac{\partial^2 \bar{\Phi}}{\partial y^2} + \frac{\partial^2 \bar{\Phi}}{\partial \bar{z}^2} = -cZ_0 \bar{\rho}_p(x, y, \bar{z}), \tag{A1}$$

with

$$\bar{\rho}_p(x, y, \bar{z}) = eN_b \hat{\rho}(\bar{z}) \frac{\exp\left(-\frac{(\rho\cos\varphi - r_0\cos\theta_0)^2 + (\rho\sin\varphi - r_0\sin\theta_0)^2}{2\sigma_x^2}\right)}{2\pi\sigma_x^2}, \tag{A2}$$

$$\hat{\rho}(\bar{z}) = \frac{\exp\left(-\frac{\bar{z}^2}{2\bar{\sigma}_z^2}\right)}{\sqrt{2\pi}\bar{\sigma}_z}, \tag{A3}$$

$$\bar{\sigma}_z = \gamma_s \sigma_z, \tag{A4}$$

where γ_s is the Lorentz-γ of the reference particle, c is light velocity, Z_0 is the impedance of free space, σ_x is the rms transverse beam size, and N_b is the number of particle per bunch. Polar coordinates are introduced as

$$x = \rho\cos\varphi, \tag{A5}$$

$$y = \rho\sin\varphi, \tag{A6}$$

and the center of the bunch on the horizontal plane is given by $(r_0\cos\theta_0, r_0\sin\theta_0)$. From now on, the condition $\sigma_x \ll a$ is assumed.

When a perfectly conductive chamber with radius a exists, the Green function $G(\vec{r}, \vec{r}')$ that satisfies the boundary condition $G = 0$ at $\rho = a$, is given by [35]

$$\begin{aligned} G(\vec{r}, \vec{r}') = &\sum_{m=0}^{\infty} \frac{\epsilon_m}{2\pi^2} \cos m(\varphi - \varphi') \\ &\times \begin{cases} \int_0^\infty d\lambda \left[K_m(\lambda\rho') - \frac{K_m(\lambda a)}{I_m(\lambda a)} I_m(\lambda\rho')\right] I_m(\lambda\rho)\cos\lambda(\bar{z} - \bar{z}'), & \text{for } \rho' > \rho, \\ \int_0^\infty d\lambda \left[K_m(\lambda\rho) - \frac{K_m(\lambda a)}{I_m(\lambda a)} I_m(\lambda\rho)\right] I_m(\lambda\rho')\cos\lambda(\bar{z} - \bar{z}'), & \text{for } \rho' < \rho, \end{cases} \end{aligned} \tag{A7}$$

where $I_m(z)$ and $K_m(z)$ are the modified Bessel functions, $\vec{r} = (\rho, \varphi, \bar{z}), \vec{r}' = (\rho', \varphi', \bar{z}'), \epsilon_m = 2 - \delta_{m0}$ and δ_{mn} is the Kronecker-δ. By using the Green function, the solution $\bar{\Phi}$ is approximated as

$$\bar{\Phi}(\rho, \varphi, \bar{z}) \simeq \int_0^\infty d\lambda \int_{-\infty}^{\infty} d\bar{z}' \int_\rho^a \rho' d\rho' \int_0^{2\pi} d\varphi' \sum_{m=0}^{\infty} \frac{cZ_0\epsilon_m}{2\pi^2} \cos m(\varphi - \varphi')$$

$$
\begin{aligned}
&\times \left[K_m(\lambda\rho') - \frac{K_m(\lambda a)}{I_m(\lambda a)} I_m(\lambda\rho')\right] I_m(\lambda\rho)\cos\lambda(\bar{z}-\bar{z}') \\
&\times eN_b \frac{\exp\left(-\frac{\bar{z}'^2}{2\bar{\sigma}_z^2}\right)}{\sqrt{2\pi}\bar{\sigma}_z} \frac{\exp\left(-\frac{(\rho'\cos\varphi' - r_0\cos\theta_0)^2 + (\rho'\sin\varphi' - r_0\sin\theta_0)^2}{2\sigma_x^2}\right)}{2\pi\sigma_x^2} \\
&+ \int_0^\infty d\lambda \int_{-\infty}^{\infty} d\bar{z}' \int_0^\rho \rho' d\rho' \int_0^{2\pi} d\varphi' \sum_{m=0}^{\infty} \frac{cZ_0\epsilon_m}{2\pi^2}\cos m(\varphi-\varphi') \\
&\times \left[K_m(\lambda\rho) - \frac{K_m(\lambda a)}{I_m(\lambda a)} I_m(\lambda\rho)\right] I_m(\lambda\rho')\cos\lambda(\bar{z}-\bar{z}') \\
&\times eN_b \frac{\exp\left(-\frac{\bar{z}'^2}{2\bar{\sigma}_z^2}\right)}{\sqrt{2\pi}\bar{\sigma}_z} \frac{\exp\left(-\frac{(\rho'\cos\varphi' - r_0\cos\theta_0)^2 + (\rho'\sin\varphi' - r_0\sin\theta_0)^2}{2\sigma_x^2}\right)}{2\pi\sigma_x^2}. \qquad \text{(A8)}
\end{aligned}
$$

By using the formulae

$$
\int_0^{2\pi} d\varphi' \cos m(\varphi-\varphi') \exp\left(\frac{\rho' r_0\cos(\varphi'-\theta_0)}{\sigma_x^2}\right) = 2\pi I_m\left(\frac{\rho' r_0}{\sigma_x^2}\right)\cos(m(\varphi-\theta_0)), \qquad \text{(A9)}
$$

$$
\frac{1}{\sqrt{2\pi}\bar{\sigma}_z}\int_{-\infty}^{\infty} d\bar{z}' \exp\left(-\frac{\bar{z}'^2}{2\bar{\sigma}_z^2}\right)\cos\lambda(\bar{z}-\bar{z}') = \exp\left(-\frac{\lambda^2\bar{\sigma}_z^2}{2}\right)\cos\lambda\bar{z}, \qquad \text{(A10)}
$$

the integrations in the azimuthal and longitudinal directions in Eq. (A8) are performed, so that we get

$$
\begin{aligned}
\bar{\Phi}(\rho,\varphi,\bar{z}) = &\int_\rho^a \rho' d\rho' \sum_{m=0}^{\infty} \frac{cZ_0\epsilon_m}{2\pi^2} eN_b \frac{\exp\left(-\frac{\rho'^2+r_0^2}{2\sigma_x^2}\right)}{\sigma_x^2} I_m\left(\frac{\rho' r_0}{\sigma_x^2}\right)\cos(m(\varphi-\theta_0)) \\
&\times \int_0^\infty d\lambda \left[K_m(\lambda\rho') - \frac{K_m(\lambda a)}{I_m(\lambda a)} I_m(\lambda\rho')\right] I_m(\lambda\rho)\cos\lambda\bar{z}\exp\left(-\frac{\lambda^2\bar{\sigma}_z^2}{2}\right) \\
&+ \int_0^\rho \rho' d\rho' \sum_{m=0}^{\infty} \frac{cZ_0\epsilon_m}{2\pi^2} eN_b \frac{\exp\left(-\frac{\rho'^2+r_0^2}{2\sigma_x^2}\right)}{\sigma_x^2} I_m\left(\frac{\rho' r_0}{\sigma_x^2}\right)\cos(m(\varphi-\theta_0)) \\
&\times \int_0^\infty d\lambda \left[K_m(\lambda\rho) - \frac{K_m(\lambda a)}{I_m(\lambda a)} I_m(\lambda\rho)\right] I_m(\lambda\rho')\cos\lambda\bar{z}\exp\left(-\frac{\lambda^2\bar{\sigma}_z^2}{2}\right). \qquad \text{(A11)}
\end{aligned}
$$

The potential $\bar{\Phi}_c$ felt at the bunch center is calculated by plugging in $\rho = r_0$ and $\varphi = \theta_0$ [26]. Figure 18 illustrates typical behavior of the potential $\bar{\Phi}_c(\bar{z}=0)$ calculated by using the beam parameters at the ramping time 15 ms in the RCS.

Here, let us expand the result for small ρ around zero. As a result, it is expressed as

$$
\bar{\Phi}_c(x,y,\bar{z}) \simeq \bar{\Phi}_{\mathrm{coh},0}(\bar{z}) + \bar{\Phi}_{\mathrm{coh},2}(\bar{z})(x^2+y^2) + \bar{\Phi}_{\mathrm{coh},4}(\bar{z})(x^2+y^2)^2, \qquad \text{(A12)}
$$

where

$$
\begin{aligned}
\bar{\Phi}_{\mathrm{coh},0}(\bar{z}) = &\frac{cZ_0 eN_b}{2\pi^2\sigma_x^2}\int_0^a d\rho'\rho' \exp\left(-\frac{\rho'^2}{2\sigma_x^2}\right)\int_0^\infty d\lambda \exp\left(-\frac{\lambda^2\bar{\sigma}_z^2}{2}\right) \\
&\times \left[K_0(\lambda\rho') - \frac{K_0(\lambda a)}{I_0(\lambda a)} I_0(\lambda\rho')\right]\cos\lambda\bar{z}, \qquad \text{(A13)}
\end{aligned}
$$

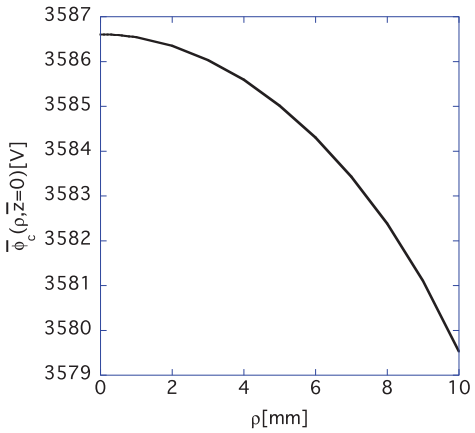

Fig. 18. Typical behavior of the potential $\bar{\Phi}_c(\bar{z}=0)$ calculated by using the beam parameters at the ramping time 15 ms in the RCS.

$$\begin{aligned}
\bar{\Phi}_{\mathrm{coh},2}(\bar{z}) = {} & \frac{cZ_0eN_b}{2\pi^2\sigma_x^2}\int_0^a d\rho'\rho'\exp\left(-\frac{\rho'^2}{2\sigma_x^2}\right)\int_0^\infty d\lambda\left(\frac{\lambda^2}{4}+\frac{\rho'^2}{4\sigma_x^4}-\frac{1}{2\sigma_x^2}\right)\exp\left(-\frac{\lambda^2\bar{\sigma}_z^2}{2}\right)\\
& \times\left[K_0(\lambda\rho')-\frac{K_0(\lambda a)}{I_0(\lambda a)}I_0(\lambda\rho')\right]\cos\lambda\bar{z}\\
& +\frac{cZ_0eN_b}{4\sigma_x^4\pi^2}\int_0^a d\rho'\rho'^2\exp\left(-\frac{\rho'^2}{2\sigma_x^2}\right)\int_0^\infty d\lambda\lambda\exp\left(-\frac{\lambda^2\bar{\sigma}_z^2}{2}\right)\\
& \times\left[K_1(\lambda\rho')-\frac{K_1(\lambda a)}{I_1(\lambda a)}I_1(\lambda\rho')\right]\cos\lambda\bar{z}-\frac{cZ_0eN_b}{8\pi^2\sigma_x^2\bar{\sigma}_z}\left(\frac{\pi}{2}\right)^{1/2}\exp\left(-\frac{\bar{z}^2}{2\bar{\sigma}_z^2}\right), \qquad \text{(A14)}
\end{aligned}$$

$$\begin{aligned}
\bar{\Phi}_{\mathrm{coh},4}(\bar{z}) = {} & \frac{cZ_0eN_b}{16\pi^2\sigma_x^2}\int_0^a d\rho'\rho'\exp\left(-\frac{\rho'^2}{2\sigma_x^2}\right)\int_0^\infty d\lambda\left(\frac{\lambda^4}{8}+\frac{\rho'^2\lambda^2}{2\sigma_x^4}+\frac{\rho'^4}{8\sigma_x^8}-\frac{\lambda^2}{\sigma_x^2}-\frac{\rho'^2}{\sigma_x^6}+\frac{1}{\sigma_x^4}\right)\\
& \times\exp\left(-\frac{\lambda^2\bar{\sigma}_z^2}{2}\right)\left[K_0(\lambda\rho')-\frac{K_0(\lambda a)}{I_0(\lambda a)}I_0(\lambda\rho')\right]\cos\lambda\bar{z}\\
& +\frac{cZ_0eN_b}{8\pi^2\sigma_x^4}\int_0^a d\rho'\exp\left(-\frac{\rho'^2}{2\sigma_x^2}\right)\int_0^\infty d\lambda\left(\frac{\rho'^4\lambda}{4\sigma_x^4}+\frac{\rho'^2\lambda^3}{4}-\frac{\rho'^2\lambda}{\sigma_x^2}\right)\exp\left(-\frac{\lambda^2\bar{\sigma}_z^2}{2}\right)\\
& \times\left[K_1(\lambda\rho')-\frac{K_1(\lambda a)}{I_1(\lambda a)}I_1(\lambda\rho')\right]\cos\lambda\bar{z}\\
& +\frac{cZ_0eN_b}{64\pi^2\sigma_x^6}\int_0^a d\rho'\exp\left(-\frac{\rho'^2}{2\sigma_x^2}\right)\rho'^3\int_0^\infty d\lambda\lambda^2\exp\left(-\frac{\lambda^2\bar{\sigma}_z^2}{2}\right)\\
& \times\left[K_2(\lambda\rho')-\frac{K_2(\lambda a)}{I_2(\lambda a)}I_2(\lambda\rho')\right]\cos\lambda\bar{z}\\
& +\frac{cZ_0eN_b}{\pi^2\sigma_x^2}\left(-\frac{(\bar{\sigma}_z^2-\bar{z}^2)}{128\bar{\sigma}_z^5}+\frac{1}{64\sigma_x^2\bar{\sigma}_z}\right)\left(\frac{\pi}{2}\right)^{1/2}\exp\left(-\frac{\bar{z}^2}{2\bar{\sigma}_z^2}\right). \qquad \text{(A15)}
\end{aligned}$$

The terms $\bar{\Phi}_{\mathrm{coh},2}(\bar{z})$ and $\bar{\Phi}_{\mathrm{coh},4}(\bar{z})$ contribute to the coherent space charge tune shift, and to the nonlinear motion of the beam, respectively.

The scalar potential Φ and the vector potential A_z in the lab-frame (ct, x, y, z) are given by

$$\Phi(x, y, z - \beta_s ct) = \gamma_s \bar{\Phi}(x, y, \gamma_s(z - \beta_s ct)), \tag{A16}$$

$$A_z(x, y, z - \beta_s ct) = \frac{\beta_s}{c} \gamma_s \bar{\Phi}(x, y, \gamma_s(z - \beta_s ct)), \tag{A17}$$

respectively, where β_s is the Lorentz-β of the reference particle.

Appendix B. Derivation of the Hamiltonian with action-angle variables including horizontal wake and space charge effects

In this section, we will obtain the Hamiltonian Eq. (B50) with action-angle variables, by successively canonically transforming Hamiltonians.

The original Hamiltonian in an electromagnetic field is approximately given by [24,25]

$$\begin{aligned} H_o = & -p_s \left(1 + \frac{x}{\rho}\right) \frac{\Delta E}{p_s \beta_s c} + \frac{p_s}{2\gamma_s^2} \left(\frac{\Delta E}{p_s \beta_s c}\right)^2 + \frac{p_x^2 + p_y^2}{2p_s} + \frac{p_s}{2} K_x(s) \left(1 - \frac{\Delta E}{E_s}\right) x^2 \\ & + \frac{p_s}{2} K_y(s) \left(1 - \frac{\Delta E}{E_s}\right) y^2 - \frac{p_s x}{E_s} F_x + \frac{e\Phi_c(x, y, s - c\beta_s t)}{\beta_s \gamma_s^2 c} \\ & - \frac{eV_{\mathrm{rf}}}{\omega_{\mathrm{RF}}} \delta_p(s) \cos\left(\omega_{\mathrm{RF}} t - \frac{hs}{R} + \varphi_s\right) + \ldots, \end{aligned} \tag{B1}$$

where φ_s is the synchronous phase; p_s is the constant momentum on the synchronous particle; $E_s = cp_s/\beta_s$ is the particle energy on the designed orbit; β_s and γ_s are the Lorentz-β and γ, respectively; ΔE is given by $\Delta E = E - E_s$; F_x is the horizontal wake force; $\delta_p(s)$ is the periodic δ-function; c is the velocity of light; K_x and K_y are the periodic focusing forces in the horizontal and vertical directions, respectively; Φ_c is the space charge potential; h is harmonic number; V_{rf} is the amplitude of the radio frequency (RF) voltage; $1/\rho$ is the local curvature around the machine; R is the average radius of the machine; and ω_{RF} is the angular frequency of the RF voltage, which is expressed as

$$\omega_{\mathrm{RF}} = \frac{c\beta_s h}{R}. \tag{B2}$$

The orbit length s is used as an independent variable. The canonical variables are (x, p_x), (y, p_y), and $(t, -E)$ for the horizontal, vertical, and the longitudinal directions, respectively. It is noticeable that the contribution from the vector potentials is included in the Hamiltonian, where the contributions from both the scalar and vector potentials are confined to the scalar potential only with Eqs. (A16) and (A17).

Using the generating function F_1,

$$\begin{aligned} F_1(x, \bar{p}_x, y, \bar{p}_y, t, -\Delta\bar{E}) = & \left(x - \frac{\Delta\bar{E}}{p_s \beta_s c} D\right) \bar{p}_x + y\bar{p}_y - t(\Delta\bar{E} + E_s) \\ & + \frac{\Delta\bar{E}}{\beta_s c} \frac{dD}{ds} x - \frac{p_s}{2} \left(\frac{\Delta\bar{E}}{p_s \beta_s c}\right)^2 D \frac{dD}{ds}, \end{aligned} \tag{B3}$$

we make a canonical transformation from the variables (x, p_x), (y, p_y), and $(t, -E)$ to $(\bar{x}, \bar{p}_x)$, $(\bar{y}, \bar{p}_y)$, and $(\bar{t}, -\Delta\bar{E})$, respectively, according to

$$p_x = \frac{\partial F_1}{\partial x} = \bar{p}_x + \frac{\Delta\bar{E}}{\beta_s c} \frac{dD}{ds}, \tag{B4}$$

$$\bar{x} = \frac{\partial F_1}{\partial \bar{p}_x} = x - \frac{\Delta\bar{E}}{p_s\beta_s c}D, \tag{B5}$$

$$p_y = \bar{p}_y, \tag{B6}$$

$$\bar{y} = y, \tag{B7}$$

$$-E = \frac{\partial F_1}{\partial t} = -\Delta\bar{E} - E_s, \tag{B8}$$

$$\bar{t} = -\frac{\partial F_1}{\partial \Delta\bar{E}} = \frac{D\bar{p}_x}{p_s\beta_s c} + t - \frac{1}{\beta_s c}\frac{dD}{ds}\bar{x}, \tag{B9}$$

where the dispersion function $D(s)$ in the horizontal direction satisfies the relation

$$\frac{d^2D}{ds^2} + K_x D = \frac{1}{\rho}. \tag{B10}$$

The new Hamiltonian H_1 is obtained as

$$\begin{aligned} H_1 \simeq{}& \frac{\bar{p}_x^2 + \bar{p}_y^2}{2p_s} + \frac{p_s}{2}\left(1 - \frac{\Delta\bar{E}}{E_s}\right)(K_x\bar{x}^2 + K_y\bar{y}^2) - \frac{p_s}{E_s}\left(\bar{x} + \frac{\Delta\bar{E}}{p_s\beta_s c}D\right)F_x \\ &+ \frac{e\Phi_c\left[\bar{x} + \frac{\Delta\bar{E}}{p_s\beta_s c}D, \bar{y}, s - c\beta_s\left(\bar{t} - \frac{D\bar{p}_x}{p_s\beta_s c} + \frac{1}{\beta_s c}\frac{dD}{ds}\bar{x}\right)\right]}{\beta_s\gamma_s^2 c} \\ &- \frac{\Delta\bar{E}}{\beta_s c} + \frac{p_s}{2\gamma_s^2}\left(\frac{\Delta\bar{E}}{p_s\beta_s c}\right)^2 - \frac{p_s}{2}\left(\frac{\Delta\bar{E}}{p_s\beta_s c}\right)^2\frac{D}{\rho} - K_x\frac{D}{p_s}\bar{x}\frac{\Delta\bar{E}^2}{c^2} - \frac{1}{2}K_x\frac{D^2}{\beta_s}\frac{\Delta\bar{E}^3}{p_s^2c^3} \\ &- \frac{eV_{\rm rf}}{\omega_{\rm RF}}\delta_p(s)\cos\left(\omega_{\rm RF}\bar{t} - \frac{hs}{R} + \varphi_s\right). \end{aligned} \tag{B11}$$

In the above derivation, the assumption is made that $D(s=0) = dD(s=0)/ds = 0$ at the RF cavity.

Next, using the generating function F_2,

$$F_2(\bar{x}, p_x, \bar{y}, p_y, W, \bar{t}) = \bar{x}\tilde{p}_x + \bar{y}\tilde{p}_y + W\left(\omega_{\rm RF}\bar{t} - \frac{hs}{R}\right), \tag{B12}$$

we make a canonical transform from $(\bar{x}, \bar{p}_x), (\bar{y}, \bar{p}_y), (\bar{t}, -\Delta\bar{E})$ to $(\tilde{x}, \tilde{p}_x), (\tilde{y}, \tilde{p}_y), (\phi_{cp}, W)$, respectively, using

$$\bar{p}_x = \frac{\partial F_2}{\partial \bar{x}} = \tilde{p}_x, \tag{B13}$$

$$\tilde{x} = \frac{\partial F_2}{\partial \tilde{p}_x} = \bar{x}, \tag{B14}$$

$$\bar{p}_y = \tilde{p}_y, \tag{B15}$$

$$\tilde{y} = \bar{y}, \tag{B16}$$

$$-\Delta\bar{E} = \frac{\partial F_2}{\partial \bar{t}} = W\omega_{\rm RF}, \tag{B17}$$

$$\phi_{cp} = \frac{\partial F_2}{\partial W} = \omega_{\rm RF}\bar{t} - \frac{hs}{R}. \tag{B18}$$

Then, the new Hamiltonian H_2 is described as

$$\begin{aligned} H_2 \simeq & \frac{\tilde{p}_x^2+\tilde{p}_y^2}{2p_s} + \frac{p_s}{2}\left(1+\frac{W\omega_{\rm RF}}{E_s}\right)(K_x\tilde{x}^2+K_y\tilde{y}^2) \\ & + \frac{e\Phi_c\left(\tilde{x}-\frac{Wh}{p_sR}D, \tilde{y}, -\frac{c\beta_s\phi_{cp}}{\omega_{\rm RF}}+\frac{D\tilde{p}_x}{p_s}-\frac{dD}{ds}\tilde{x}\right)}{\beta_s\gamma_s^2 c} \\ & - \frac{p_s}{E_s}\left(\tilde{x}-\frac{\omega_{\rm RF}W}{p_s\beta_s c}D\right)F_x - K_x\frac{D}{p_s}\tilde{x}\frac{W^2\omega_{\rm RF}^2}{c^2} + \frac{1}{2}K_x\frac{D^2}{\beta_s}\frac{W^3\omega_{\rm RF}^3}{p_s^2c^3} \\ & + \left(\frac{1}{\gamma_s^2}-\frac{D}{\rho}\right)\frac{h^2}{2R^2p_s}W^2 - \frac{eV_{\rm rf}}{\omega_{\rm RF}}\delta_p(s)\cos(\phi_{cp}+\varphi_s), \end{aligned} \tag{B19}$$

where Eq. (B2) is used.

By extracting the Hamiltonian $H_{3,L}$ for the synchrotron oscillation, we obtain

$$H_{3,L} \equiv -\frac{\eta h^2}{2R^2p_s}W^2 + \frac{eV_{\rm rf}\cos\varphi_s}{4\pi R\omega_{\rm RF}}\phi_{cp}^2 = -\frac{\eta h^2}{2R^2p_s}W^2 - \frac{E_sc^2\beta_s^4}{2\eta\omega_0R\omega_{\rm RF}^2}\left(\frac{\nu_{s0}}{R}\right)^2\phi_{cp}^2, \tag{B20}$$

where the synchrotron tune ν_{s0} is given by

$$\nu_{s0} = \frac{1}{\beta_s}\left(-\frac{\eta he V_{\rm rf}\cos\varphi_s}{2\pi E_s}\right)^{1/2}. \tag{B21}$$

Accordingly, Eq. (B19) is rewritten as

$$\begin{aligned} H_2 \simeq & H_{3,L} + \frac{\tilde{p}_x^2+\tilde{p}_y^2}{2p_s} + \frac{p_s}{2}\left(1+\frac{W\omega_{\rm RF}}{E_s}\right)(K_x\tilde{x}^2+K_y\tilde{y}^2) \\ & + \frac{e\Phi_c\left(\tilde{x}-\frac{Wh}{p_sR}D, \tilde{y}, -\frac{c\beta_s\phi_{cp}}{\omega_{\rm RF}}+\frac{D\tilde{p}_x}{p_s}-\frac{dD}{ds}\tilde{x}\right)}{\beta_s\gamma_s^2 c} \\ & - \frac{p_s}{E_s}\left(\tilde{x}-\frac{\omega_{\rm RF}W}{p_s\beta_s c}D\right)F_x - K_x\frac{D}{p_s}\tilde{x}\frac{W^2\omega_{\rm RF}^2}{c^2} + \frac{1}{2}K_x\frac{D^2}{\beta_s}\frac{W^3\omega_{\rm RF}^3}{p_s^2c^3} \\ & + \left(\frac{1}{\gamma_s^2}-\frac{D}{\rho}\right)\frac{h^2}{2R^2p_s}W^2 - \frac{eV_{\rm rf}}{\omega_{\rm RF}}\delta_p(s)\cos(\phi_{cp}+\varphi_s) \\ & + \frac{\eta h^2}{2R^2p_s}W^2 - \frac{eV_{\rm rf}\cos\varphi_s}{4\pi R\omega_{\rm RF}}\phi_{cp}^2. \end{aligned} \tag{B22}$$

Before describing the Hamiltonian in terms of action-angle variables, let us continue to make the canonical transformations from $(\tilde{x},\tilde{p}_x)$, $(\tilde{y},\tilde{p}_y)$ to $(\bar{\tilde{x}},\bar{\tilde{p}}_x)$, $(\bar{\tilde{y}},\bar{\tilde{p}}_y)$, respectively, which are generated by the function F_3:

$$F_3(\bar{\tilde{x}},\tilde{p}_x,\bar{\tilde{y}},\tilde{p}_y) = -\frac{\bar{\tilde{x}}\tilde{p}_x}{\sqrt{p_s}} - \frac{\bar{\tilde{y}}\tilde{p}_y}{\sqrt{p_s}}. \tag{B23}$$

The canonical transformations are expressed as

$$\bar{\tilde{p}}_x = \frac{\tilde{p}_x}{\sqrt{p_s}}, \qquad \tilde{x} = \frac{\bar{\tilde{x}}}{\sqrt{p_s}}, \tag{B24}$$

$$\bar{\tilde{p}}_y = \frac{\tilde{p}_y}{\sqrt{p_s}}, \qquad \tilde{y} = \frac{\bar{\bar{y}}}{\sqrt{p_s}}. \tag{B25}$$

The new Hamiltonian H_3 is divided as

$$H_3 = H_{3,L} + H_{3,T} + \Delta H_{3,T} + \Delta H_{3,L}, \tag{B26}$$

where $H_{3,L}$ is given by Eq. (B20), and

$$H_{3,T} \equiv \frac{\bar{\bar{p}}_x^2 + \bar{\bar{p}}_y^2}{2} + \frac{1}{2}(K_x \bar{\bar{x}}^2 + K_y \bar{\bar{y}}^2) - \frac{p_s}{E_s}\left(\frac{\bar{\bar{x}}}{\sqrt{p_s}} - \frac{\omega_{\rm RF} W}{p_s \beta_s c} D\right) F_x, \tag{B27}$$

$$\Delta H_{3,T} = \frac{W\omega_{\rm RF}}{2E_s}(K_x \bar{\bar{x}}^2 + K_y \bar{\bar{y}}^2) + \frac{e\Phi_c\left(\frac{\bar{\bar{x}}}{\sqrt{p_s}} - \frac{Wh}{p_s R} D, \frac{\bar{\bar{y}}}{\sqrt{p_s}}, -\frac{c\beta_s \phi_{cp}}{\omega_{\rm RF}} + \frac{D\bar{\bar{p}}_x}{\sqrt{p_s}} - \frac{dD}{ds}\frac{\bar{\bar{x}}}{\sqrt{p_s}}\right)}{\beta_s \gamma_s^2 c}$$
$$- K_x \frac{D}{p_s}\frac{\bar{\bar{x}}}{\sqrt{p_s}}\frac{W^2\omega_{\rm RF}^2}{c^2} + \frac{1}{2}K_x \frac{D^2}{\beta_s}\frac{W^3\omega_{\rm RF}^3}{p_s^2 c^3}, \tag{B28}$$

$$\Delta H_{3,L} = \left(\frac{1}{\gamma_s^2} - \frac{D}{\rho}\right)\frac{h^2}{2R^2 p_s} W^2 - \frac{eV_{\rm rf}}{\omega_{\rm RF}}\delta_p(s)\cos(\phi_{cp} + \varphi_s) + \frac{\eta h^2}{2R^2 p_s} W^2 - \frac{eV_{\rm rf}\cos\varphi_s}{4\pi R\omega_{\rm RF}}\phi_{cp}^2. \tag{B29}$$

For the longitudinal motion, let us consider the generating function

$$F(\phi_{cp}, \phi_L, s) = -\frac{cp_s\beta_s\nu_{s0}}{2h^2|\eta|\omega_0}\phi_{cp}^2 \tan\left(\phi_L - \frac{\pi}{2}\right), \tag{B30}$$

which gives

$$\phi_{cp} = \left(\frac{2J_L h^2|\eta|\omega_0}{cp_s\beta_s\nu_{s0}}\right)^{1/2}\sin\phi_L, \tag{B31}$$

$$W = \left(\frac{2J_L\nu_{s0}cp_s\beta_s}{|\eta|h^2\omega_0}\right)^{1/2}\cos\phi_L. \tag{B32}$$

Consequently, the Hamiltonian is written as

$$H_{3,L} + \Delta H_{3,L} = -\frac{|\eta|}{\eta}\frac{\nu_{s0}}{R}J_L + \frac{|\eta|}{\eta}\frac{\nu_{s0}}{R}J_L\sin^2\phi_L$$
$$- \frac{eV_{\rm rf}}{\omega_{\rm RF}}\delta_p(s)\cos\left(\left(\frac{2J_L h^2|\eta|\omega_0}{cp_s\beta_s\nu_{s0}}\right)^{1/2}\sin\phi_L + \varphi_s\right). \tag{B33}$$

To extract the Twiss parameters dependence from the transverse variables $(\bar{\bar{x}}, \bar{\bar{p}}_x)$ and $(\bar{\bar{y}}, \bar{\bar{p}}_y)$, we consider the canonical transformations generated by the function F_4:

$$F_4(\bar{\bar{x}}, \psi_x, \bar{\bar{y}}, \psi_y, s) = -\frac{\bar{\bar{x}}^2}{2\beta_x(s)}\left[\tan\left(\psi_x + \phi_x(s) - \frac{Q_x}{R}s\right) + \alpha_x(s)\right]$$
$$- \frac{\bar{\bar{y}}^2}{2\beta_y(s)}\left[\tan\left(\psi_y + \phi_y(s) - \frac{Q_y}{R}s\right) + \alpha_y(s)\right], \tag{B34}$$

$$\phi_x(s) = \int^s \frac{ds}{\beta_x(s)}, \tag{B35}$$

$$\phi_y(s) = \int^s \frac{ds}{\beta_y(s)}. \tag{B36}$$

We obtain the canonical transformations from $(\bar{\bar{x}}, \bar{\bar{p}}_x)$, $(\bar{\bar{y}}, \bar{\bar{p}}_y)$ to (J_x, ψ_x), (J_y, ψ_y), respectively, as

$$\bar{\bar{p}}_x = \frac{\partial F_4}{\partial \bar{\bar{x}}} = -\frac{\bar{\bar{x}}}{\beta_x(s)}\left[\tan\left(\psi_x + \phi_x(s) - \frac{Q_x}{R}s\right) + \alpha_x(s)\right], \tag{B37}$$

$$J_x = -\frac{\partial F_4}{\partial \psi_x} = \frac{\bar{\bar{x}}^2}{2\beta_x(s)\cos^2\left(\psi_x + \phi_x(s) - \frac{Q_x}{R}s\right)}, \tag{B38}$$

$$\bar{\bar{p}}_y = -\frac{\bar{\bar{y}}}{\beta_y(s)}\left[\tan\left(\psi_y + \phi_y(s) - \frac{Q_y}{R}s\right) + \alpha_y(s)\right], \tag{B39}$$

$$J_y = \frac{\bar{\bar{y}}^2}{2\beta_y(s)\cos^2\left(\psi_y + \phi_y(s) - \frac{Q_y}{R}s\right)}, \tag{B40}$$

where the Twiss parameters satisfy

$$\frac{d^2}{ds^2}\sqrt{\beta_i} + K_i\sqrt{\beta_i} - \frac{1}{(\sqrt{\beta_i})^3} = 0, \tag{B41}$$

$$\alpha_i = -\frac{1}{2}\frac{d\beta_i}{ds}, \tag{B42}$$

$$\beta_i\gamma_{s,i} - \alpha_i^2 = 1, \tag{B43}$$

and i denotes x or y.

Thus, the new Hamiltonian H_4 is expressed as

$$H_4 \simeq H_{4,0} + \Delta H_4, \tag{B44}$$

where

$$\begin{aligned} H_{4,0} = {} & \frac{Q_x J_x}{R} + \frac{Q_y J_y}{R} - \frac{\eta}{|\eta|}\frac{\nu_{s0} J_L}{R} \\ & - \frac{2\beta_s}{c}\left(\left(\frac{\beta_x(s)J_x}{2p_s}\right)^{1/2}\cos\left(\psi_x + \phi_x(s) - \frac{Q_x}{R}s\right) - \frac{D(s)}{\beta_s}\left(\frac{\omega_0\nu_{s0}J_L}{2E_s|\eta|}\right)^{1/2}\cos\phi_L\right)F_x, \end{aligned} \tag{B45}$$

$$\begin{aligned} \Delta H_4 = {} & K_x\beta_x(s)J_x\left(\frac{2J_L\nu_{s0}\beta_s^2\omega_0}{|\eta|E_s}\right)^{1/2}\cos\phi_L\cos^2\left(\psi_x + \phi_x(s) - \frac{Q_x}{R}s\right) \\ & + K_y\beta_y(s)J_y\left(\frac{2J_L\nu_{s0}\beta_s^2\omega_0}{|\eta|E_s}\right)^{1/2}\cos\phi_L\cos^2\left(\psi_y + \phi_y(s) - \frac{Q_y}{R}s\right) + \frac{e\Phi_c(X,Y,Z)}{\beta_s\gamma_s^2 c} \\ & - K_x D\left(\frac{2\beta_x(s)J_x}{c\beta_s E_s}\right)^{1/2}\frac{2J_L\omega_0\nu_{s0}\beta_s}{|\eta|}\cos\left(\psi_x + \phi_x(s) - \frac{Q_x}{R}s\right)\cos^2\phi_L \\ & + K_x\sqrt{2}\frac{D^2\omega_0^3}{\sqrt{E_s}c}\left(\frac{J_L\nu_{s0}}{|\eta|\omega_0}\right)^{3/2}\cos^3\phi_L \end{aligned}$$

$$+\frac{|\eta|}{\eta}\frac{\nu_{s0}}{R}J_L\sin^2\phi_L-\frac{eV_{\rm rf}}{\omega_{\rm RF}}\delta_p(s)\cos\left(\left(\frac{2J_Lh^2|\eta|\omega_0}{cp_s\beta_s\nu_{s0}}\right)^{1/2}\sin\phi_L+\varphi_s\right), \tag{B46}$$

$$X=\left(\frac{2\beta_x(s)J_x}{p_s}\right)^{1/2}\cos\left(\psi_x+\phi_x(s)-\frac{Q_x}{R}s\right)-\frac{h}{p_sR}D\left(\frac{2J_L\nu_{s0}cp_s\beta_s}{|\eta|h^2\omega_0}\right)^{1/2}\cos\phi_L, \tag{B47}$$

$$Y=\left(\frac{2\beta_y(s)J_y}{p_s}\right)^{1/2}\cos\left(\psi_y+\phi_y(s)-\frac{Q_y}{R}s\right), \tag{B48}$$

$$\begin{aligned}Z=&\frac{c\beta_s}{\omega_{\rm RF}}\left(\frac{2J_Lh^2|\eta|\omega_0}{cp_s\beta_s\nu_{s0}}\right)^{1/2}\sin\phi_L\\&+\frac{D}{\sqrt{p_s}}\left(\frac{2J_x}{\beta_x(s)}\right)^{1/2}\left[\alpha_x(s)\cos\left(\psi_x+\phi_x(s)-\frac{Q_x}{R}s\right)+\sin\left(\psi_x+\phi_x(s)-\frac{Q_x}{R}s\right)\right]\\&+\frac{dD}{ds}\left(\frac{2\beta_x(s)J_x}{p_s}\right)^{1/2}\cos\left(\psi_x+\phi_x(s)-\frac{Q_x}{R}s\right).\end{aligned} \tag{B49}$$

The application of the canonical perturbation theory (see, e.g., Ref. [36]) for the Hamiltonian and neglecting the higher-order terms lead to the new Hamiltonian H:

$$H\simeq Q_xJ_x+Q_yJ_y+J_L\nu_{s0}+U_x+Y', \tag{B50}$$

with its independent variable $\theta=s/R$, where

$$U_x=-R\frac{2\beta_s}{c}\left(\left(\frac{\beta_x(s)J_x}{2p_s}\right)^{1/2}\cos\left(\psi_x+\phi_x(s)-\frac{Q_x}{R}s\right)-\frac{D(s)}{\beta_s}\left(\frac{\omega_0\nu_{s0}J_L}{2E_s|\eta|}\right)^{1/2}\cos\phi_L\right)F_x, \tag{B51}$$

$$\begin{aligned}Y'=&\frac{eR}{8\pi^3\beta_s\gamma_s^2c}\int_0^{2\pi}d\psi_x\int_0^{2\pi}d\psi_y\int_0^{2\pi}d\phi_L\\&\times\Phi_c\left[\left(\frac{2\beta_x(s)J_x}{p_s}\right)^{1/2}\cos\psi_x-\frac{D(s)}{R}\left(\frac{2J_L\nu_{s0}c\beta_s}{|\eta|p_s\omega_0}\right)^{1/2}\cos\phi_L,\left(\frac{2\beta_y(s)J_y}{p_s}\right)^{1/2}\cos\psi_y,\right.\\&\frac{c}{h}\left(\frac{2J_L|\eta|}{\omega_0E_s\nu_{s0}}\right)^{1/2}\sin\phi_L+\frac{D(s)}{\sqrt{p_s}}\left(\frac{2J_x}{\beta_x(s)}\right)^{1/2}(\alpha_x(s)\cos\psi_x+\sin\psi_x)\\&\left.+\frac{dD}{ds}\left(\frac{2\beta_x(s)J_x}{p_s}\right)^{1/2}\cos\psi_x\right],\end{aligned} \tag{B52}$$

U_x and Y' are the effect of the horizontal wake and the space charge forces, respectively.

Here, we consider a rather nonrelativistic condition, namely, a long bunch beam in the ring with the conditions

$$\left(\frac{2\beta_x(s)J_x}{p_s}\right)^{1/2}\ll\frac{|D|}{R}\left(\frac{2J_L\nu_{s0}c\beta_s}{|\eta|p_s\omega_0}\right)^{1/2}, \tag{B53}$$

$$\left|\frac{D}{\sqrt{p_s}}\left(\frac{2J_x}{\beta_x(s)}\right)^{1/2}(\alpha_x(s)+1)+\frac{dD}{ds}\left(\frac{2\beta_x(s)J_x}{p_s}\right)^{1/2}\right|\ll\frac{c}{h}\left(\frac{2J_L|\eta|}{\omega_0E_s\nu_{s0}}\right)^{1/2}. \tag{B54}$$

In this case, the function Y' is approximated as

$$Y' = Y'_{\mathrm{coh},0}(J_L) + Y'_{\mathrm{coh},2}(J_L)\left(\frac{\beta_x(s)J_x}{p_s} + \frac{\beta_y(s)J_y}{p_s}\right) + Y'_{\mathrm{coh},4}(J_L)\left(\frac{3\beta_x^2(s)J_x^2}{2} + \frac{3\beta_y^2(s)J_y^2}{2} + 2\beta_x(s)\beta_y(s)J_xJ_y\right), \tag{B55}$$

where

$$Y'_{\mathrm{coh},0}(J_L) = \frac{eRZ_0eN_b}{2\pi^2\beta_s\gamma_s\sigma_x^2}\int_0^a d\rho'\rho'\exp\left(-\frac{\rho'^2}{2\sigma_x^2}\right)\int_0^\infty d\lambda\exp\left(-\frac{\lambda^2\gamma_s^2\sigma_z^2}{2}\right) \times\left[K_0(\lambda\rho') - \frac{K_0(\lambda a)}{I_0(\lambda a)}I_0(\lambda\rho')\right]J_0\left[\gamma_s\frac{\lambda c}{h}\left(\frac{2J_L|\eta|}{\omega_0E_s\nu_{s0}}\right)^{1/2}\right], \tag{B56}$$

$$\begin{aligned} Y'_{\mathrm{coh},2}(J_L) = {} & \frac{eRZ_0eN_b}{2\pi^2\sigma_x^2\beta_s\gamma_s}\int_0^a d\rho'\rho'\exp\left(-\frac{\rho'^2}{2\sigma_x^2}\right)\int_0^\infty d\lambda\left(\frac{\lambda^2}{4} + \frac{\rho'^2}{4\sigma_x^4} - \frac{1}{2\sigma_x^2}\right) \\ & \times\exp\left(-\frac{\lambda^2\gamma_s^2\sigma_z^2}{2}\right)\left[K_0(\lambda\rho') - \frac{K_0(\lambda a)}{I_0(\lambda a)}I_0(\lambda\rho')\right]J_0\left[\gamma_s\frac{\lambda c}{h}\left(\frac{2J_L|\eta|}{\omega_0E_s\nu_{s0}}\right)^{1/2}\right] \\ & + \frac{eRZ_0eN_b}{4\sigma_x^4\pi^2\beta_s\gamma_s}\int_0^a d\rho'\rho'^2\exp\left(-\frac{\rho'^2}{2\sigma_x^2}\right)\int_0^\infty d\lambda\lambda\exp\left(-\frac{\lambda^2\gamma_s^2\sigma_z^2}{2}\right) \\ & \times\left[K_1(\lambda\rho') - \frac{K_1(\lambda a)}{I_1(\lambda a)}I_1(\lambda\rho')\right]J_0\left[\gamma_s\frac{\lambda c}{h}\left(\frac{2J_L|\eta|}{\omega_0E_s\nu_{s0}}\right)^{1/2}\right] \\ & - \frac{eRZ_0eN_b}{8\pi^2\beta_s\gamma_s^2\sigma_x^2\sigma_z}\left(\frac{\pi}{2}\right)^{1/2}\exp\left(-\frac{c^2J_L|\eta|}{2\sigma_z^2h^2\omega_0E_s\nu_{s0}}\right)I_0\left(\frac{c^2J_L|\eta|}{2\sigma_z^2h^2\omega_0E_s\nu_{s0}}\right), \end{aligned} \tag{B57}$$

$$\begin{aligned} Y'_{\mathrm{coh},4}(J_L) = {} & \frac{eRZ_0eN_b}{16\pi^2\sigma_x^2\beta_s\gamma_sp_s^2}\int_0^a d\rho'\rho'\exp\left(-\frac{\rho'^2}{2\sigma_x^2}\right)J_0\left[\gamma_s\frac{\lambda c}{h}\left(\frac{2J_L|\eta|}{\omega_0E_s\nu_{s0}}\right)^{1/2}\right] \\ & \times\int_0^\infty d\lambda\left(\frac{\lambda^4}{8} + \frac{\rho'^2\lambda^2}{2\sigma_x^4} + \frac{\rho'^4}{8\sigma_x^8} - \frac{\lambda^2}{\sigma_x^2} - \frac{\rho'^2}{\sigma_x^6} + \frac{1}{\sigma_x^4}\right)\exp\left(-\frac{\lambda^2\gamma_s^2\sigma_z^2}{2}\right) \\ & \times\left[K_0(\lambda\rho') - \frac{K_0(\lambda a)}{I_0(\lambda a)}I_0(\lambda\rho')\right] \\ & + \frac{eRZ_0eN_b}{8\pi^2\sigma_x^4\beta_s\gamma_sp_s^2}\int_0^a d\rho'\exp\left(-\frac{\rho'^2}{2\sigma_x^2}\right)J_0\left[\gamma_s\frac{\lambda c}{h}\left(\frac{2J_L|\eta|}{\omega_0E_s\nu_{s0}}\right)^{1/2}\right] \\ & \times\int_0^\infty d\lambda\left(\frac{\rho'^4\lambda}{4\sigma_x^4} + \frac{\rho'^2\lambda^3}{4} - \frac{\rho'^2\lambda}{\sigma_x^2}\right)\exp\left(-\frac{\lambda^2\gamma_s^2\sigma_z^2}{2}\right)\left[K_1(\lambda\rho') - \frac{K_1(\lambda a)}{I_1(\lambda a)}I_1(\lambda\rho')\right] \\ & + \frac{eRZ_0eN_b}{64\pi^2\sigma_x^6\beta_s\gamma_sp_s^2}\int_0^a d\rho'\exp\left(-\frac{\rho'^2}{2\sigma_x^2}\right)\rho'^3\int_0^\infty d\lambda\lambda^2\exp\left(-\frac{\lambda^2\gamma_s^2\sigma_z^2}{2}\right) \\ & \times\left[K_2(\lambda\rho') - \frac{K_2(\lambda a)}{I_2(\lambda a)}I_2(\lambda\rho')\right]J_0\left[\gamma_s\frac{\lambda c}{h}\left(\frac{2J_L|\eta|}{\omega_0E_s\nu_{s0}}\right)^{1/2}\right] \\ & + \frac{eRZ_0eN_b}{\beta_s\gamma_s^2\pi^2\sigma_x^2p_s^2}\left(\frac{\pi}{2}\right)^{1/2}\exp\left(-\frac{c^2J_L|\eta|}{2h^2\omega_0E_s\nu_{s0}\sigma_z^2}\right) \end{aligned}$$

$$\times\left[\left(-\frac{1}{128\gamma_s^2\sigma_z^3}+\frac{1}{64\sigma_x^2\sigma_z}+\frac{c^2J_L|\eta|}{128\gamma_s^2\sigma_z^5h^2\omega_0E_s\nu_{s0}}\right)\right.$$
$$\left.\times I_0\left(\frac{c^2J_L|\eta|}{2h^2\omega_0E_s\nu_{s0}\sigma_z^2}\right)-\frac{c^2J_L|\eta|I_1(\frac{c^2J_L|\eta|}{2h^2\omega_0E_s\nu_{s0}\sigma_z^2})}{128\gamma_s^2\sigma_z^5h^2\omega_0E_s\nu_{s0}}\right]. \quad \text{(B58)}$$

Finally, they are simplified to Eqs. (7), (8), and (9) as in the text, under a typical parameter region.

References

[1] Japan Proton Accelerator Research Complex. Available at http://j-parc.jp/index-e.html, date last accessed January 9, 2017.
[2] Y. Shobuda, Y. Irie, and S. Igarashi, Phys. Rev. ST Accel. Beams **12**, 032401 (2009).
[3] Y. Shobuda and Y. Irie, JPS Conf. Proc. **8**, 012003 (2015).
[4] M. Kinsho, D. Nishizawa, Y. Saito, H. Suzuki, and H. Yokomizo, J. Vac. Sci. Technol. A **20**, 829 (2002); M. Kinsho, N. Ogiwara, Y. Saito, and Z. Kabeya, Proc. PAC 2005, Knoxville, Tennessee, p. 2604 (2005).
[5] Y. Shobuda, Y. H. Chin, and K. Takata, Phys. Rev. ST Accel. Beams **17**, 091001 (2014).
[6] A. W. Chao, *Physics of Collective Beam Instabilities in High Energy Accelerators* (Wiley, New York, 1993).
[7] A. W. Chao and M. Tigner (Eds.), *Handbook of Accelerator Physics and Engineering* (World Scientific Publishing Co. Pte. Ltd, Singapore, 1999).
[8] Y. Shobuda and K. Yokoya, Phys. Rev. E **66**, 056501 (2002).
[9] Y. Shobuda, Y. H. Chin, and K. Takata, Phys. Rev. ST Accel. Beams **12**, 094401 (2009).
[10] Y. Shobuda, Nucl. Instrum. Methods A **741**, 177 (2014).
[11] Y. H. Chin, S. Lee, K. Takata, T. Toyama, Y. Shobuda, and H. Tsutsui, Proc. HB2006, Tsukuba, Japan, p. 125 (2006).
[12] Y. Shobuda, N. Hayashi, T. Takayanagi, T. Toyama, and Y. Irie, Proc. IPAC2013, Shanghai, China, p. 1742 (2013).
[13] Y. Shobuda, P. K. Saha, T. Toyama, M. Yamamoto, Y. H. Chin, and Y. Irie, Proc. HB2014, Michigan, USA, p. 369 (2014).
[14] Y. H. Chin, K. Takata, T. Toyama, Y. Shobuda and J. Kamiya, Proc. HB2008, Nashville, Tennessee, USA, p. 40 (2008).
[15] Y. Shobuda, Y. Irie, T. Toyama, J. Kamiya, and M. Watanabe, Nucl. Instrum. Methods A **713**, 52 (2013).
[16] N. Ogiwara, J. Kamiya, Y. Shobuda, M. Kinsho, and O. Koizumi, Proc. IPAC2013, Shanghai, China, p. 3321 (2013).
[17] Y. Shobuda, Y. Irie, and T. Toyama, Nucl. Instrum. Methods A **691**, 135 (2012).
[18] F. Sacherer, in *1st International School of Particle Accelerators "Ettore Majorana" - Theoretical Aspects of the Behaviour of Beams in Accelerators and Storage Rings*, ed. M. Hildred (CERN, Geneva, 1977), p. 175.
[19] F. Sacherer, CERN/SI-BR/72-5 (1972).
[20] M. Blaskiewicz, Phys. Rev. ST Accel. Beams **1**, 044201 (1998).
[21] A. Burov, Phys. Rev. ST Accel. Beams **12**, 044202 (2009); **12**, 109901 (2009) [erratum].
[22] Y. H. Chin, A. W. Chao, and M. M. Blaskiewicz, Rev. Accel. Beams **19**, 014201 (2016).
[23] Y. Shobuda, Beam no ukeru Impedance to Beam no Fuanteisei no Riron, in OHO2010 (Tsukuba, KEK, 2010) (in Japanese).
[24] T. Suzuki, KEK Report 96-10 (1996).
[25] H. Okamoto, *Kôsoku Ion Beam No Kesshôka* (Kyôritsu-shuppan, Tokyo, 2000) (in Japanese).
[26] H. Wiedemann, *Particle Accelerator Physics II* (Springer, Berlin, New York, 1999), 2nd ed.
[27] M. Abramowitz and I. Stegun, *Handbook of Mathematical Functions–with Formulas, Graphs, and Mathematical Tables* (Dover, New York, 1974).
[28] P. K. Saha, Y. Shobuda, H. Hotchi, N. Hayashi, T. Takayanagi, H. Harada, and Y. Irie, Phys. Rev. ST Accel. Beams **12**, 040403 (2009).
[29] P. K. Saha, H. Harada, N. Hayashi, K. Horino, H. Hotchi, M. Kinsho, T. Takayanagi, N. Tani, T. Togashi, T. Ueno, and Y. Yamazaki, Phys. Rev. ST Accel. Beams **16**, 120102 (2013).

[30] H. Hotchi, Proc. HB2008, Nashville, Tennessee, USA, p. 6 (2008).
[31] T. Kamei and M. Kihara, *Kasokuki Kagaku* (Maruzen, Tokyo, 1993) (in Japanese).
[32] P. K. Saha, Y. Shobuda, H. Hotchi, H. Harada, N. Hayashi, F. Tamura, and M. Yamamoto, Proc. IPAC2014, Dresden, Germany, p. 1683 (2014).
[33] P. K. Saha, Y. Shobuda, H. Hotchi, H. Harada, N. Hayashi, F. Tamura, and M. Yamamoto, Proc. IPAC2013, Shanghai, China, p. 521 (2013).
[34] P. K. Saha, Y. Shobuda, H. Hotchi, H. Harada, N. Hayashi, M. Kinsho, M. Nomura, F. Tamura, N. Tani, Y. Watanabe, and M. Yamamoto, Proc. IPAC2016, Busan, Korea, p. 589 (2016).
[35] T. Imamura, *Butsuri to Green Kansû* (Iwanami, Tokyo, 1994) (in Japanese).
[36] A. Lichtenberg and M. Lieberman, *Regular and Chaotic Dynamics* (Springer, New York, 1992).